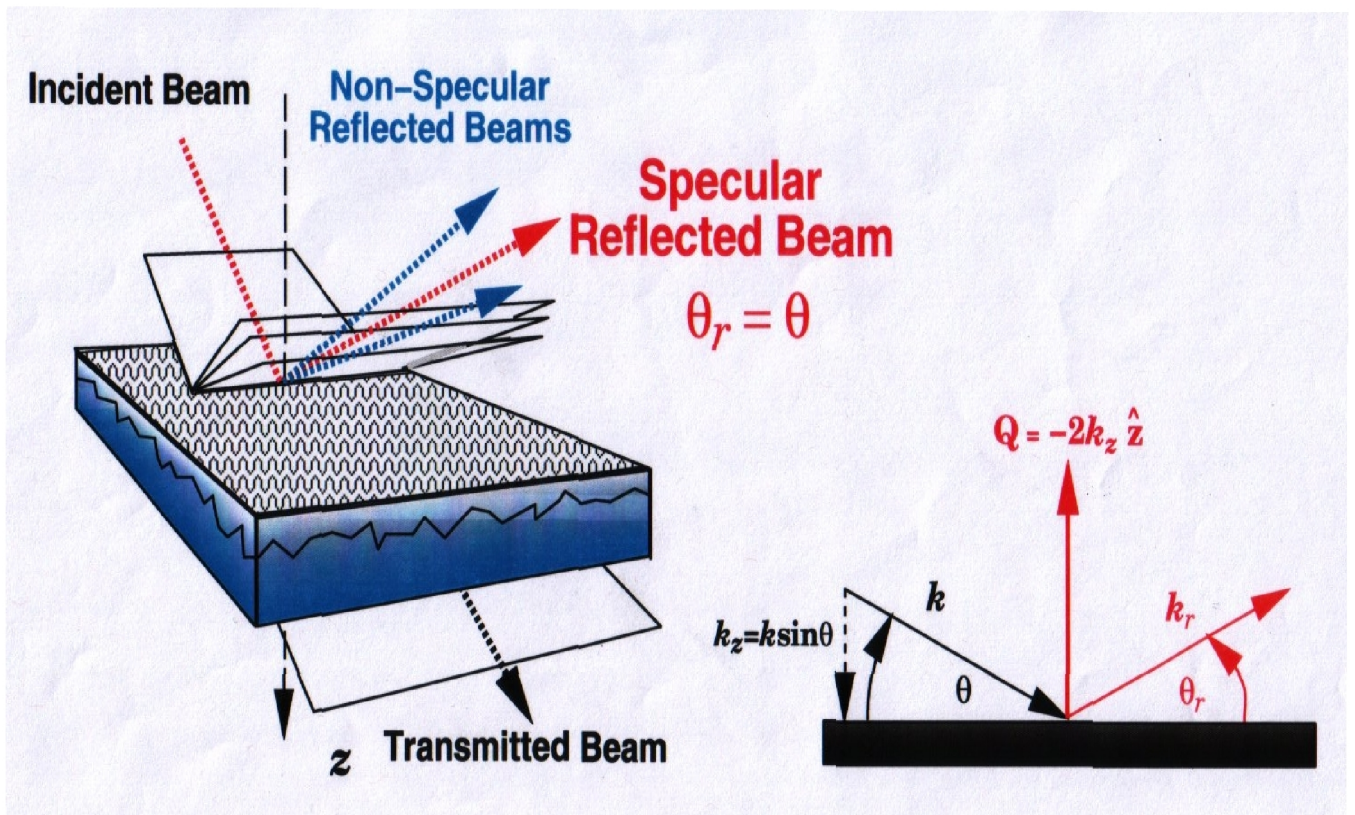


# School on Neutron Scattering

*NIST Center for Neutron Research*

## Neutron Reflectometry

27 June 2016



(Figure courtesy of Norm Berk)

C.F.Majkrzak, *NIST Center for Neutron Research*,  
Gaithersburg, MD

**Part 1: Basic reflectometry concepts**

**Part 2: Neutron wave characteristics and coherence**

**Part 3: The phase problem, direct inversion and simultaneous fitting**

**Part 4: Applications of NR to studies of the nano-scale structure of thin film materials**

**Appendices**

**Bibliography**

# Part 1: Basic Reflectometry Concepts

- <> general notes
- <> probing structure beneath the surface boundary
- <> scattering length density (SLD) depth profiles
- <> specular reflection from a *flat* object
- <> wave/particle behavior
- <> coherence length -- plane waves and wave packets
- <> spatial and Q resolutions
- <> non-specular scattering
- <> polarized neutrons and magnetic materials

# Principal Uses and Advantages of Neutron Reflectometry:

- \* For the specular condition, provides the chemical (isotopic) scattering length density (SLD) depth profile along the surface normal with a spatial resolution approaching half a nanometer.
- \* With polarized neutrons, provides the *vector* magnetization depth profile of a ferromagnetic material.
- \* Isotopic contrast, particularly applicable to hydrogen and deuterium.
- \* A non-destructive probe which can penetrate macroscopic distances through single crystalline substrates, making possible reflection studies of films in contact with liquids within a closed cell.
- \* As a consequence of the relatively weak interaction between the neutron and material, a remarkably accurate theoretical description of the reflection process and quantitative analysis of the data is possible, although the Born approximation is often not valid and an “exact” or “dynamical” formulation is required.

# Importance of Sample System Preparation

- > The great success in using neutron reflection/diffraction to study thin film systems of hard condensed matter, in particular the structures and fundamental interactions in magnetic materials, is largely due to the ability to tailor, with atomic-layer accuracy and precision, single-crystalline, layered sandwiches and superlattices (using vapor deposition techniques such as molecular beam epitaxy in ultra-high vacuum). Advances in film deposition techniques and lithography continue at a remarkable rate.
- > Similarly, neutron reflectometry in principle can be applied as a probe to further our understanding of the structure and function of molecules in lipid membranes, of relevance in biology and bioengineering, when comparable control over the fabrication of model systems is achieved. Great progress has been made toward realizing this goal in practice. However, we are still at a relatively early stage of development in our ability to engineer soft condensed matter films on atomic and nanometer scales. Progress can be expected as efforts in creating and manipulating membrane / molecular systems accelerates.
- > Employing phase-sensitive methods in reflectivity measurements ensures a unique scattering length density (SLD) depth profile. Additional application of hydrogen / deuterium substitution techniques and comparison with molecular dynamics calculations assures a correspondingly high degree of certainty of obtaining an unambiguous chemical composition depth profile.

# Why is specular neutron reflectometry so special?

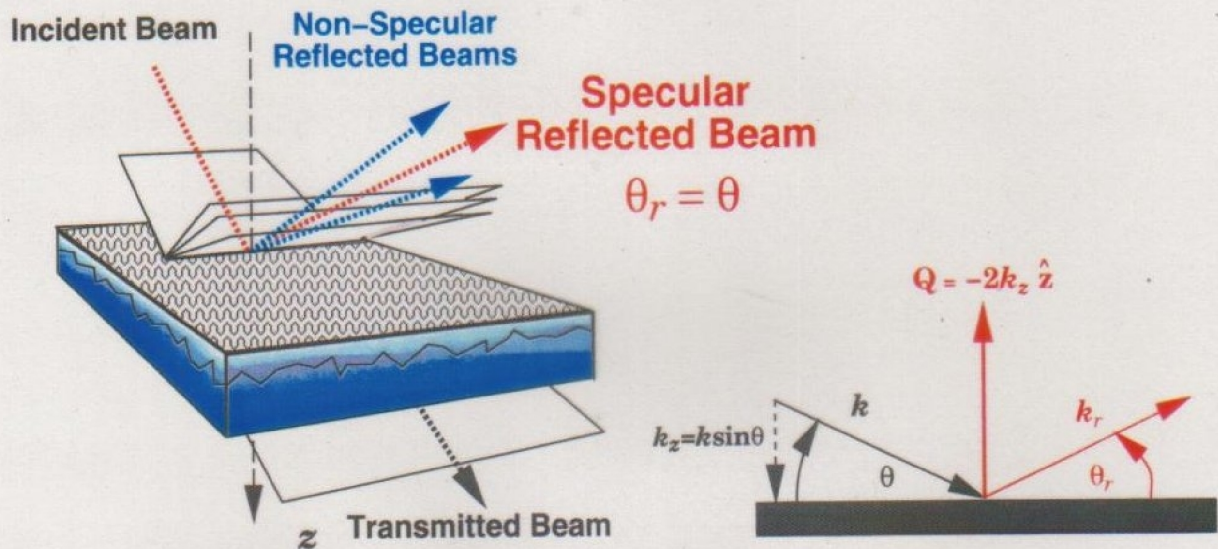
<> Neutron reflectometry (NR) is a valuable probe of the structure of both hard and soft condensed matter in thin film or multilayered form -- particularly for hydrogenous and magnetic materials. NR can see *beneath* the surface and provide quantitative structural information from *everywhere within* the film on a nanometer scale.

<> Both “forward” and “inverse” scattering problems for specular neutron reflection are mathematically solvable, exactly, from first-principles quantum theory. The mathematically unique solutions are thus far only possible in one dimension and for non-absorbing potentials of finite extent.

<> Phase-sensitive neutron specular reflectometry, employing references, enables direct inversion of composite reflectivity data sets to yield a unique scattering length density depth profile for an “unknown” film of interest, without fitting or any adjustable parameters.

<> The spatial resolution and accuracy of the SLD profile thereby obtained is limited only by the statistical uncertainty in the measured reflected intensities and truncation of the reflectivity data sets at the maximum value of wavevector transfer attainable.

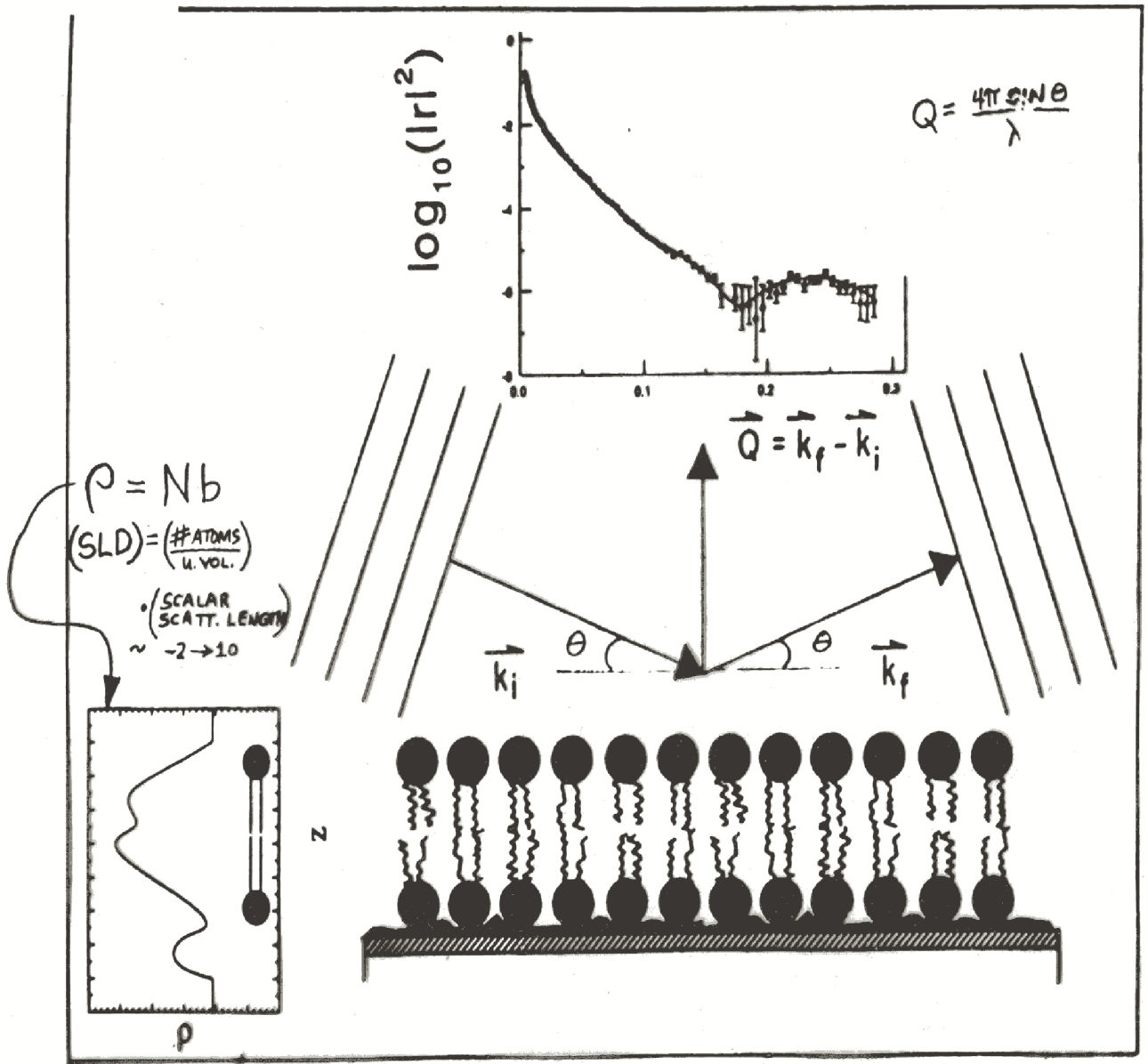
$$\text{Reflectivity} = \frac{\text{Number of reflected neutrons}}{\text{Number of incident neutrons}} = |r|^2$$



**Specular reflection:**  $\bar{\rho}(z) = \langle \rho(x, y, z) \rangle_{xy}$

**Non-Specular reflection:**  $\Delta\rho(x, y, z) = \rho(x, y, z) - \bar{\rho}(z)$

(AFTER N.F. BERK ET AL.)



Overview of the specular reflection method to determine the scattering length density (SLD) depth profile along the mean normal to the surface. The reflectivity (reflected intensity / incident intensity)  $|r|^2$  is measured as a function of wavevector transfer  $Q$ .  $|r(Q)|^2$  can then be fit to a model of the SLD profile from which the corresponding chemical composition depth profile can be inferred. Note that the SLD obtained in this manner corresponds to the in-plane average value (i.e., the plane perpendicular to  $Q$ ).

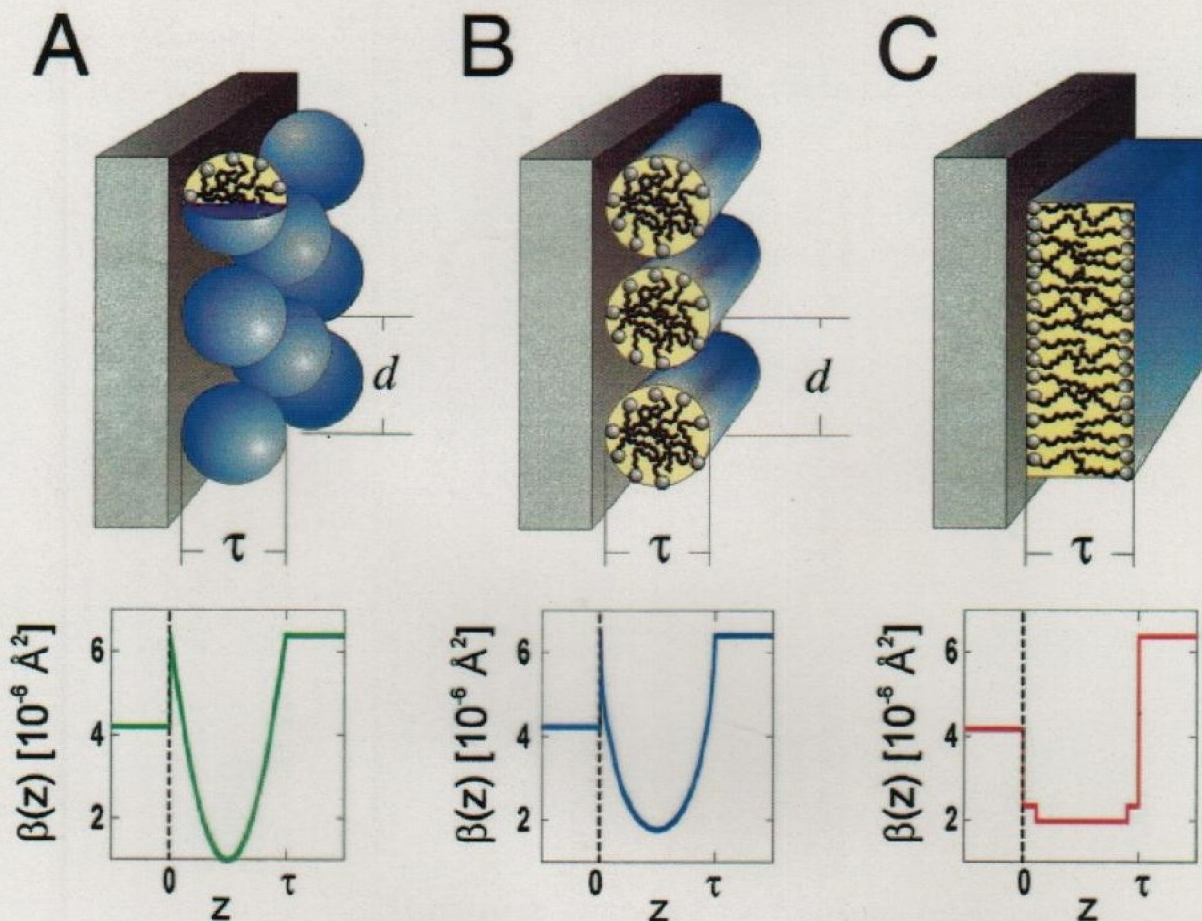


FIG. 1. (Color) Schematic diagram of adsorbed layer structures consisting of (A) spherical micelles, (B) cylindrical micelles, and (C) a bilayer, including the film thickness  $\tau$  and interaggregate spacing  $d$ . Also shown are examples of neutron scattering length density profiles normal to the interface,  $\beta(z)$ , corresponding to each structure at the quartz/D<sub>2</sub>O interface at a fractional surface coverage of 0.55. The head-group and alkyl tails of the surfactants have different scattering length densities, but because of the arrangement of the molecules this is only apparent in the bilayer  $\beta(z)$ .

single-crystal quartz block and reflected from the quartz-solution interface were recorded as a function of angle of incidence. The off-specular background, including any signal due to scattering from the bulk solution [15], was subtracted to give the reflection coefficient of the surfactant-coated interface. All solutions used were above their critical micelle

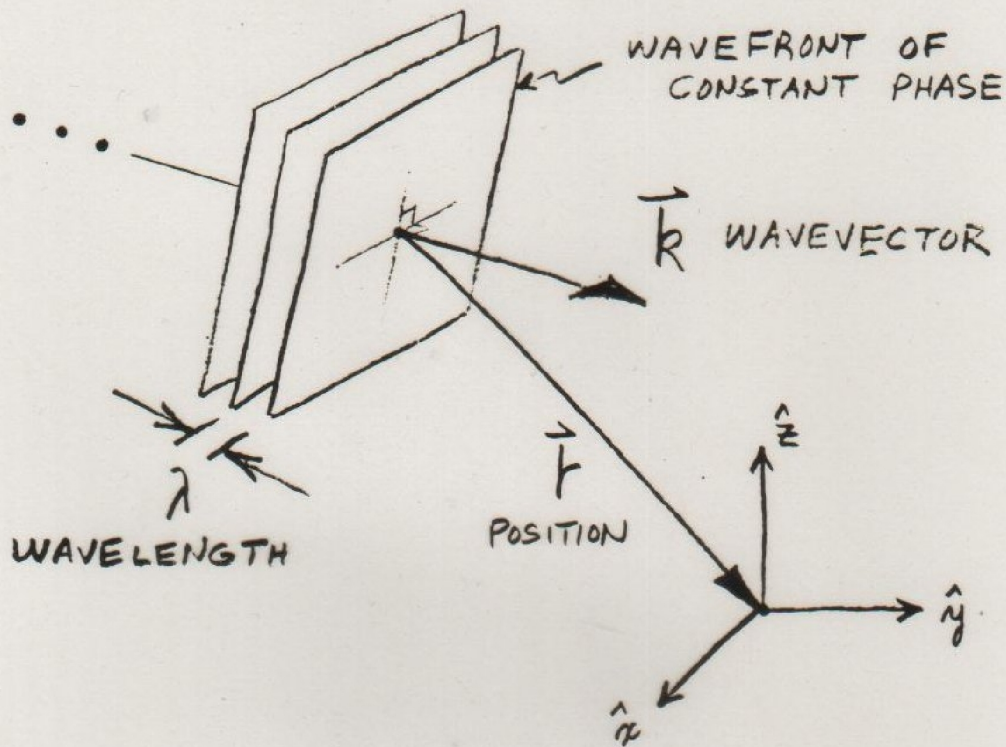
or aggregation concentration, a condition which leads to a saturated adsorbed film at the solid-solution interface.

The cationic surfactant tetradecyltrimethylammonium bromide (TTAB) forms nearly spherical micellar aggregates consisting of approximately 80 molecules in bulk solution. Small angle neutron-scattering measurements [16] give mi-



FIG. 2.  $200 \times 200\text{-nm}^2$  AFM tip deflection images of (A) spherical TTAB aggregates adsorbed onto quartz from water solution, (B) cylindrical TTAB aggregates adsorbed onto quartz from an aqueous 200mM NaBr solution, and (C) planar DDAB bilayer adsorbed onto quartz from water solution. Long-wavelength undulations visible in (B) and (C) arise from roughness in the underlying quartz.

# THE NEUTRON AS A PLANE WAVE PROPAGATING IN FREE SPACE



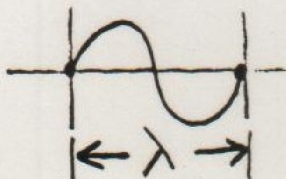
WAVEFUNCTION

$$\Psi \propto e^{i \vec{k}_0 \cdot \vec{r}}$$

$$\begin{cases} \vec{k}_0 = k_{0x} \hat{x} + k_{0y} \hat{y} + k_{0z} \hat{z} \\ \vec{r} = x \hat{x} + y \hat{y} + z \hat{z} \end{cases}$$

FOR  $\vec{k}_0$  ALONG  $\hat{z}$ , FOR EXAMPLE,

$$\Psi \propto \cos(k_{0z} z) + i \sin(k_{0z} z)$$



$$= \left( \frac{2\pi}{\lambda} z \right)$$

$$|\Psi|^2 \propto \text{PROBABILITY OF THE NEUTRON BEING THERE}$$

FOR ELASTIC INTERACTIONS  
TOTAL ENERGY OF THE  
NEUTRON IS CONSTANT

$$\begin{aligned}\text{TOTAL ENERGY} &= \text{KINETIC ENERGY} \\ &+ \text{POTENTIAL ENERGY} \\ &= \text{CONSTANT}\end{aligned}$$

WAVE EQUATION OF MOTION  
(SCHRÖDINGER EQUATION)

$$\underbrace{\left[ \frac{-\hbar^2}{2m} \nabla^2 \right]}_{\text{K.E.}} + \underbrace{V(\vec{r})}_{\text{P.E.}} = \underbrace{E}_{\text{T.E.}} \Psi$$

$$\nabla^2 = \frac{\partial^2}{\partial x^2} + \frac{\partial^2}{\partial y^2} + \frac{\partial^2}{\partial z^2}$$

IN VACUUM

$$\text{K.E.}_0 = \frac{\hbar^2 k_0^2}{2m}$$

IN THE CONTINUUM LIMIT

$$V(\vec{r}) = \frac{2\pi\hbar^2}{m} \sum_{j=1} N_j b_j = \frac{2\pi\hbar^2}{m} \rho$$

NUMBER OF ATOMS  
OF TYPE  $j$  PER UNIT  
VOLUME

SCATTERING LENGTH  
DENSITY (SLD)

COHERENT  
SCATTERING LENGTH  
OF ATOM  $j$  —

$$b = \underbrace{\text{Re}b}_{\text{SCATTERING}} + i \underbrace{\text{Im}b}_{\text{ABSORPTION}}$$

IN VACUUM

$$E_0 = \frac{\hbar^2 k_0^2}{2m} + 0$$

IN A MATERIAL MEDIUM

$$E = \frac{\hbar^2 k^2}{2m} + \frac{2\pi\hbar^2}{m} \rho$$

CONSERVATION OF ENERGY REQUIRES  $E_0 = E$   
SO THAT

$$k^2 = k_0^2 - 4\pi\rho$$

∴ THEREFORE

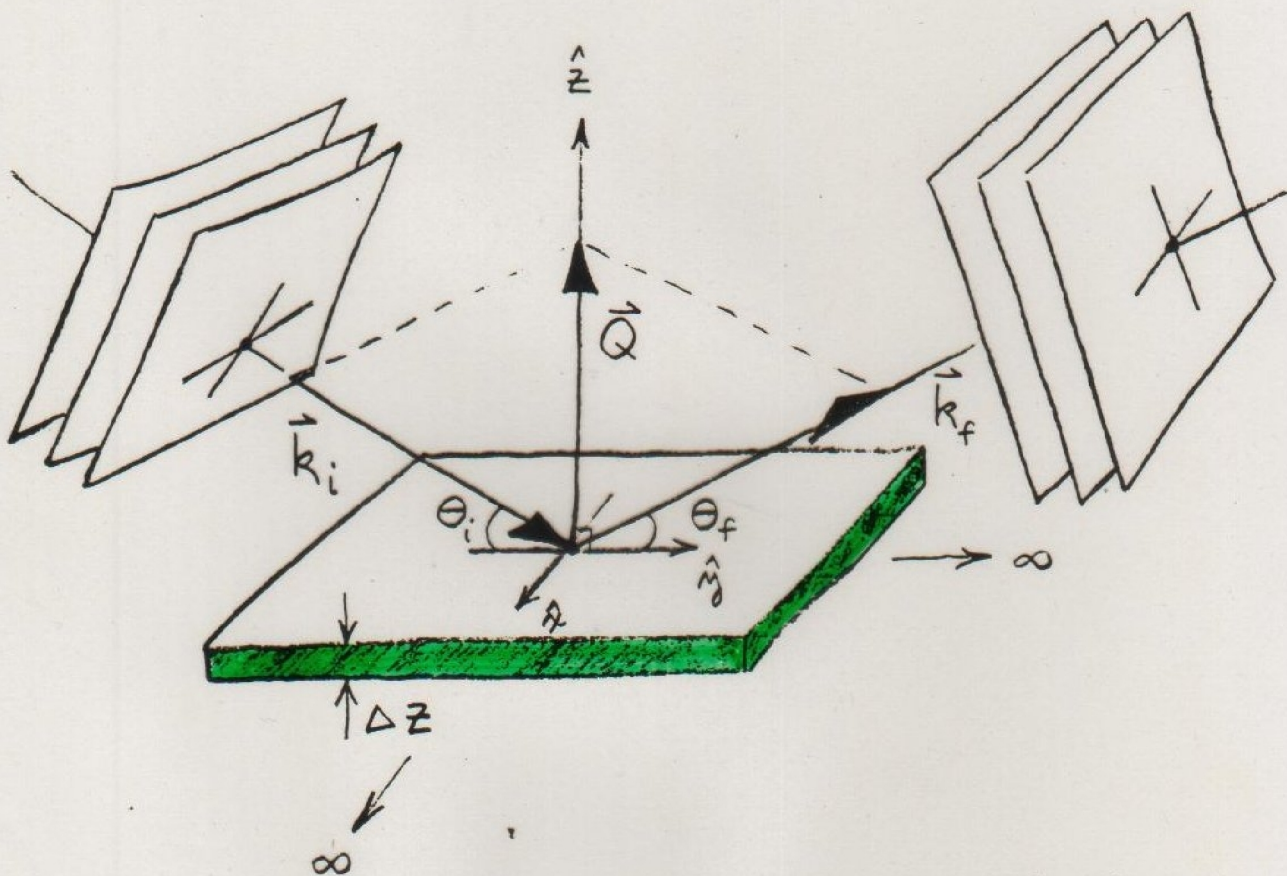
$$[\nabla^2 + k^2] \Psi = 0$$

CAN THEN DEFINE A REFRACTIVE INDEX  $n \equiv \frac{k}{k_0}$

OR

$$n^2 = 1 - \frac{4\pi\rho}{k_0^2}$$

# REFLECTION FROM AN IDEAL FILM OR SLAB OF MATERIAL



WAVEVECTOR TRANSFER  $\vec{Q} = \vec{k}_f - \vec{k}_i$

$\rho = \rho(z)$  ONLY

EXPANDING  $k^2 = k_0^2 - 4\pi\rho$ ,

$$k_x^2 + k_y^2 + k_z^2 + 4\pi\rho = k_{0x}^2 + k_{0y}^2 + k_{0z}^2.$$

NOW IF  $\rho = \rho(z)$  ONLY, THEN

$$\frac{\partial \rho}{\partial x} \text{ AND } \frac{\partial \rho}{\partial y}, \text{ WHICH ARE}$$

PROPORTIONAL TO THE GRADIENTS OF THE POTENTIAL OR FORCES IN THE RESPECTIVE DIRECTIONS, ARE EQUAL TO ZERO. THUS, NO FORCE ACTS ALONG THESE DIRECTIONS TO CHANGE  $k_x$  AND  $k_y$ . THEN

$$k_x = k_{0x} \text{ AND } k_y = k_{0y} \text{ ARE}$$

"CONSTANTS OF THE MOTION".

SUBSTITUTING  $\underline{\Psi}(\vec{r}) = e^{ik_{0x}x} e^{ik_{0y}y} \psi(z)$

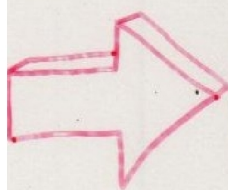
INTO  $[\nabla^2 + k^2]\underline{\Psi} = 0$  GIVES

$$\left[ \frac{\partial^2}{\partial z^2} + k_z^2 \right] \psi(z) = 0$$

$$\text{AND } \therefore k_z^2 = k_{0z}^2 - 4\pi\rho(z).$$

BECAUSE THERE IS NO CHANGE IN THE POTENTIAL IN THE X- OR Y- DIRECTIONS, THERE CAN BE NO MOMENTUM CHANGE IN THESE DIRECTIONS EITHER

THE IDEAL SLAB GEOMETRY WITH  $\rho = \rho(z)$  ONLY GIVES RISE TO THE COHERENT "SPECULAR" REFLECTION OF A PLANE WAVE WHICH IS DESCRIBED BY A ONE-DIMENSIONAL WAVE EQUATION:

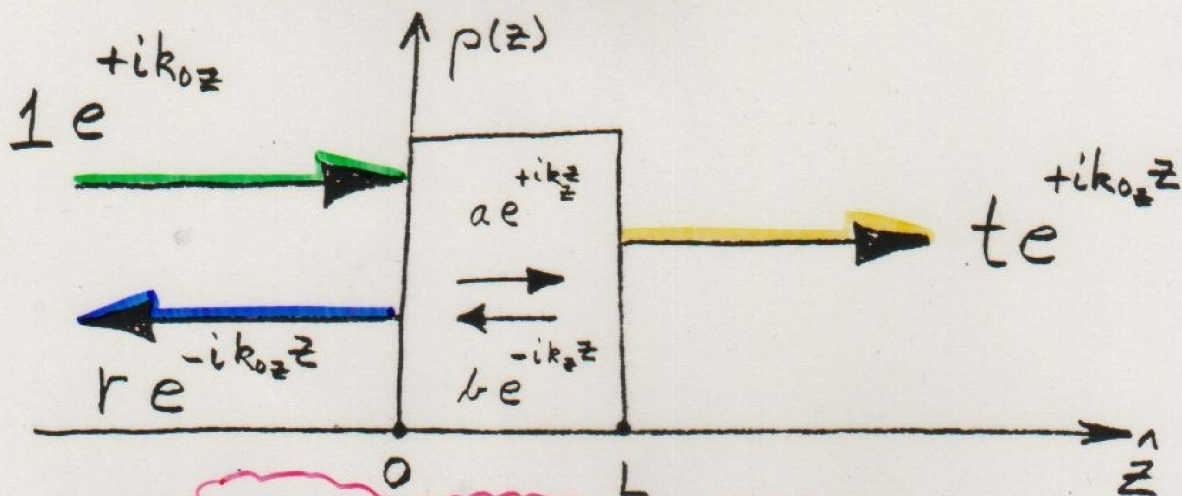


$$\left[ \frac{\partial^2}{\partial z^2} + k_{0z}^2 - 4\pi\rho(z) \right] \psi(z) = 0$$

IN THIS CASE  $\theta_i = \theta_f \equiv \theta$ ,

$$|\vec{k}_i| = |\vec{k}_f| \quad \text{AND} \quad Q = 2k \sin\theta \\ = 2k_z$$

$$\text{ALSO, } n_z^2 \equiv 1 - \frac{4\pi\rho(z)}{k_{0z}^2}$$

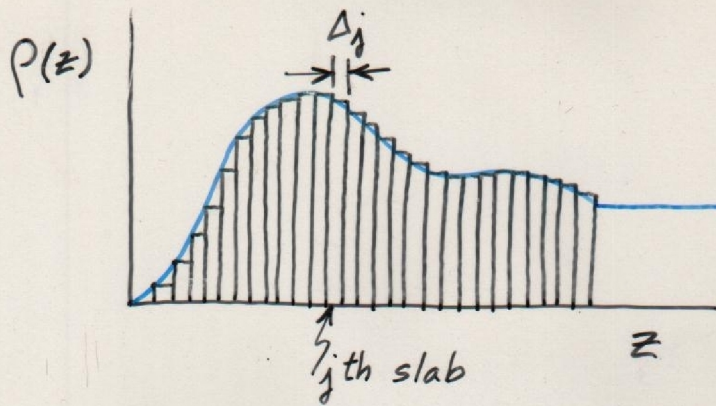


$$\frac{\partial^2 \Psi(z)}{\partial z^2} + k_z^2 \Psi(z) = 0$$

CONSERVATION OF MOMENTUM  
AND PARTICLE NUMBER  
REQUIRE THAT  $\frac{\partial \Psi(z)}{\partial z}$  AND  $\Psi(z)$

BE CONTINUOUS AT THE  
BOUNDARIES  $z=0$  &  $z=L$

$$\begin{pmatrix} t \\ it \end{pmatrix} e^{ik_0z L} = \begin{pmatrix} A & B \\ C & D \end{pmatrix} \begin{pmatrix} 1+r \\ i(1-r) \end{pmatrix}$$



$$\begin{pmatrix} A & B \\ C & D \end{pmatrix} = \begin{pmatrix} a_N & b_N \\ c_N & d_N \end{pmatrix} \begin{pmatrix} a_{N-1} & b_{N-1} \\ c_{N-1} & d_{N-1} \end{pmatrix} \cdots \begin{pmatrix} a_2 & b_2 \\ c_2 & d_2 \end{pmatrix} \begin{pmatrix} a_1 & b_1 \\ c_1 & d_1 \end{pmatrix}$$

$$\begin{pmatrix} a_j & b_j \\ c_j & d_j \end{pmatrix} = \begin{pmatrix} \cos S_j & \frac{1}{m_{zj}} \sin S_j \\ -m_{zj} \sin S_j & \cos S_j \end{pmatrix}$$

$$\begin{aligned} S_j &= k_{0z} m_{zj} \Delta_j \\ &= k_{zj} \Delta_j \end{aligned}$$

The elements A, B, C, and D of the so-called “transfer” matrix which relates the reflection, transmission, and incident wave amplitudes -- r, t, and 1, respectively -- contain all of the information about the SLD composition of the film. The transfer matrix can be constructed of a product of matrices, each of which corresponds to one successive “slice” of the film over which the SLD is taken to be a constant value. Thus, any arbitrary profile can be rendered -- and to whatever spatial resolution is needed by making the thicknesses of the slices small enough.

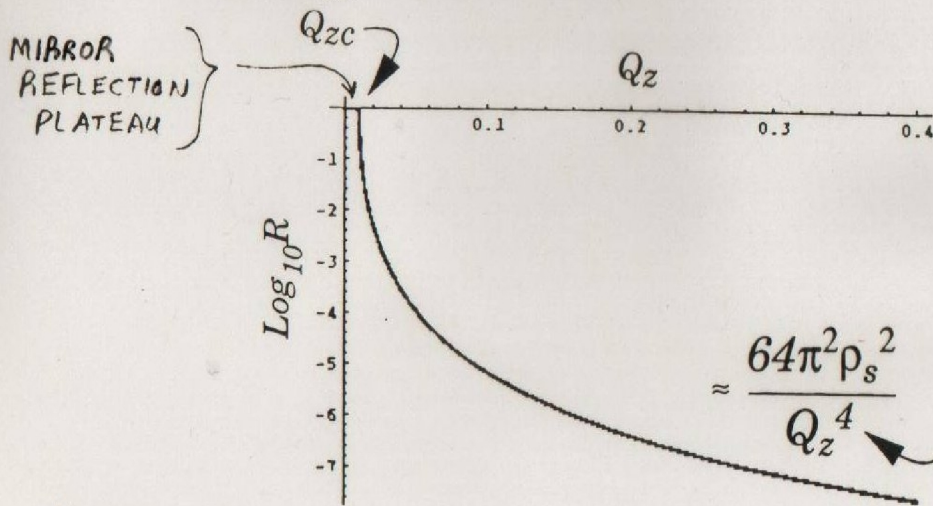
# Fresnel Reflectivity



$$|r_F|^2 \equiv R_F(Q_z)$$

$$R_F(Q_z) = \frac{1 - \sqrt{1 - \frac{Q_{zc}^2}{Q^2}}}{1 + \sqrt{1 - \frac{Q_{zc}^2}{Q^2}}}$$

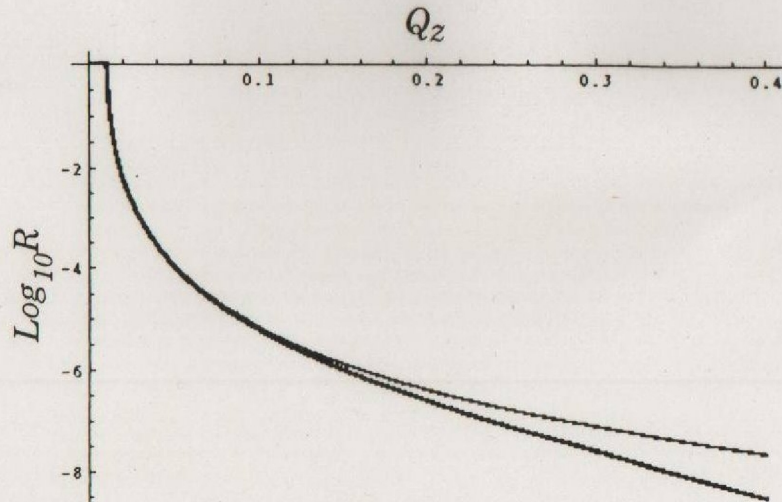
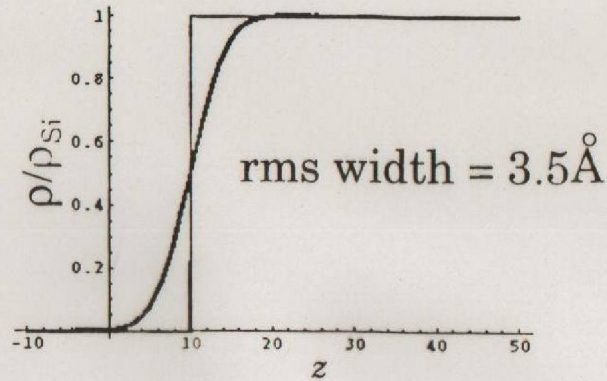
For  $Q_z < Q_{zc}$ ,  $R_F = 1$ .



$$Q_{zc} = \text{SQRT}(16 * \pi * \rho) \text{ (Courtesy of Norm Berk)}$$

## "Soft" substrate

Smooth transition:  
interlayer diffusion  
roughness

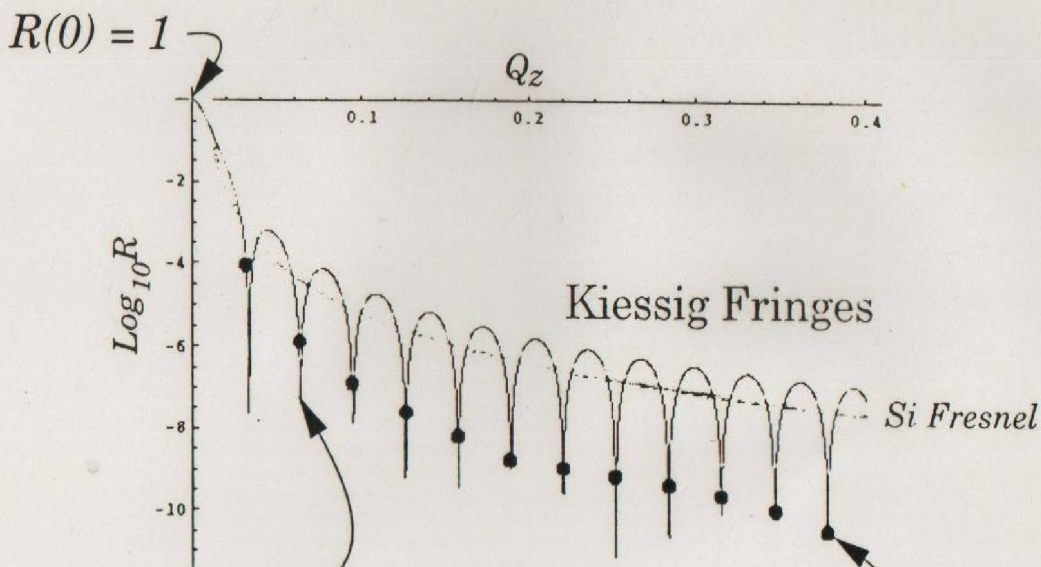
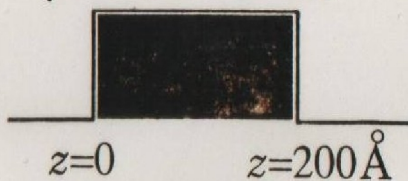


(N.F. BERK)

For an interface that is not perfectly "sharp", the reflectivity falls off with increasing  $Q$  faster than  $1/(Q^4)$ .

# Uniform slab

$$\rho = 2.07 \cdot 10^{-6} \text{ \AA}^{-2}$$



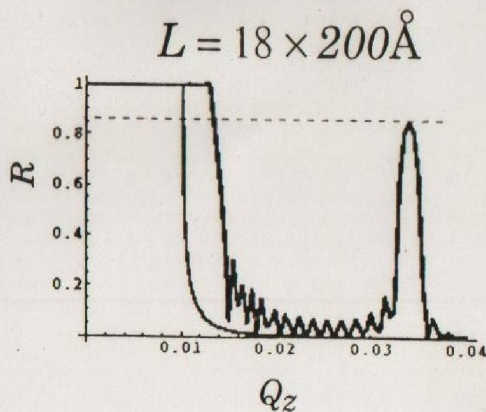
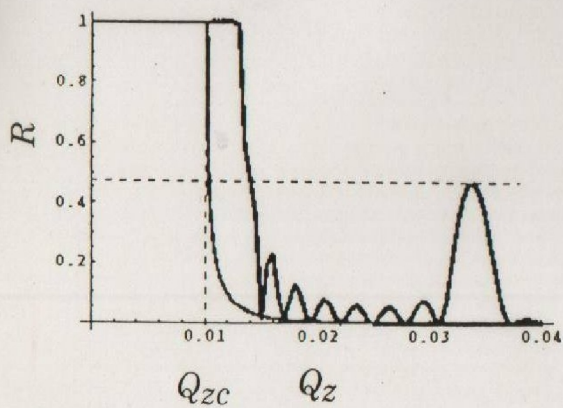
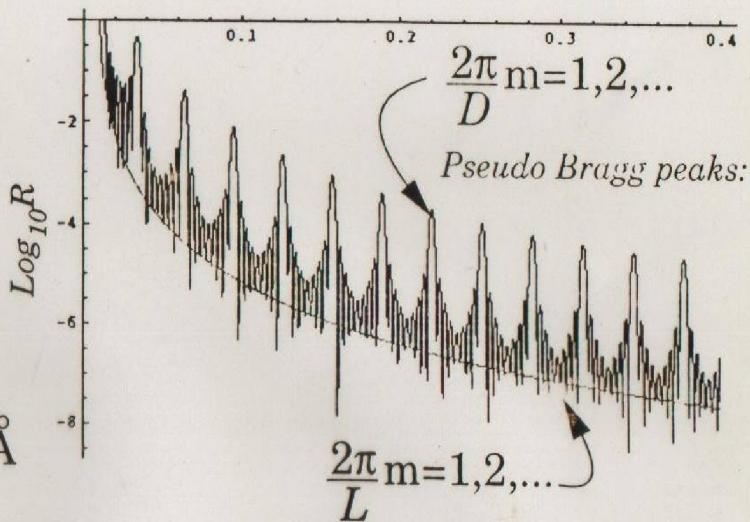
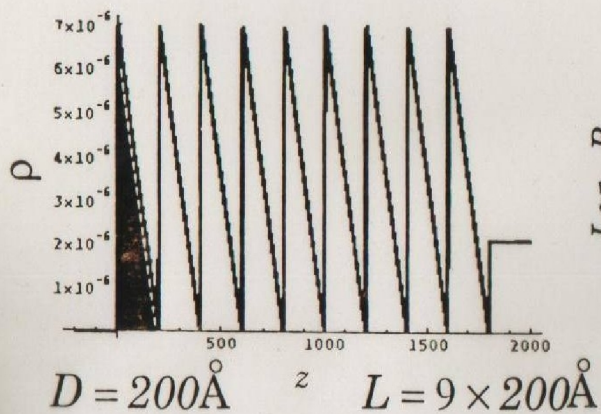
$$\sqrt{Q_z^2 - 16\pi\rho} = \frac{2\pi}{L} m = 1, 2, \dots$$

$$\frac{2\pi}{L} m = 1, 2, \dots$$

(Kinematical)

(N.F. BERK)

# Multilayer on Si



(N.F.BERK)

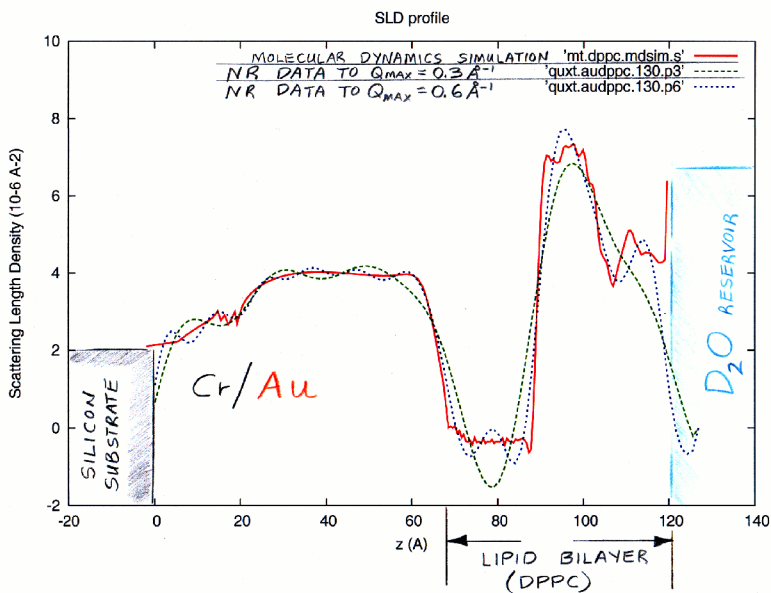
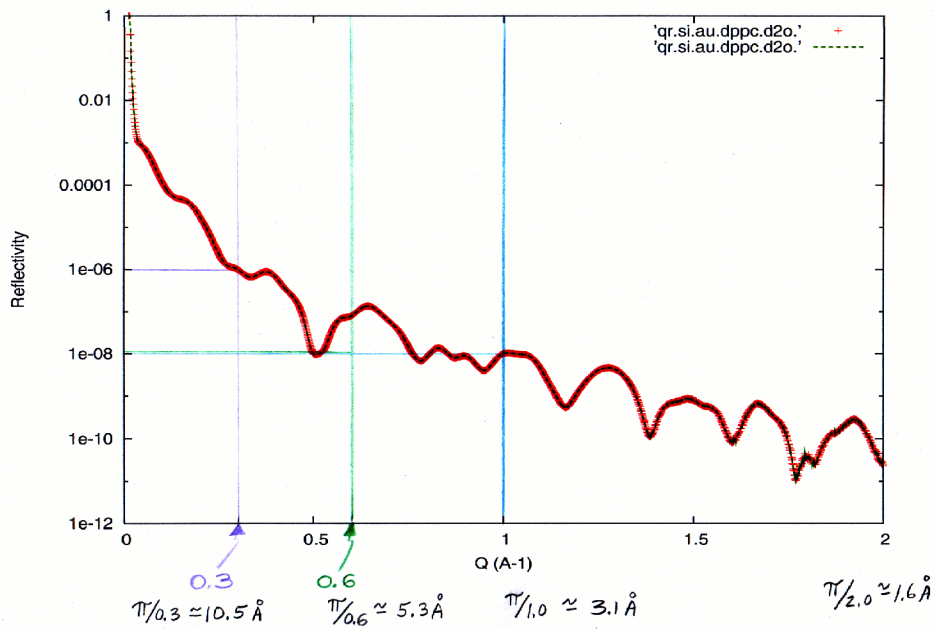
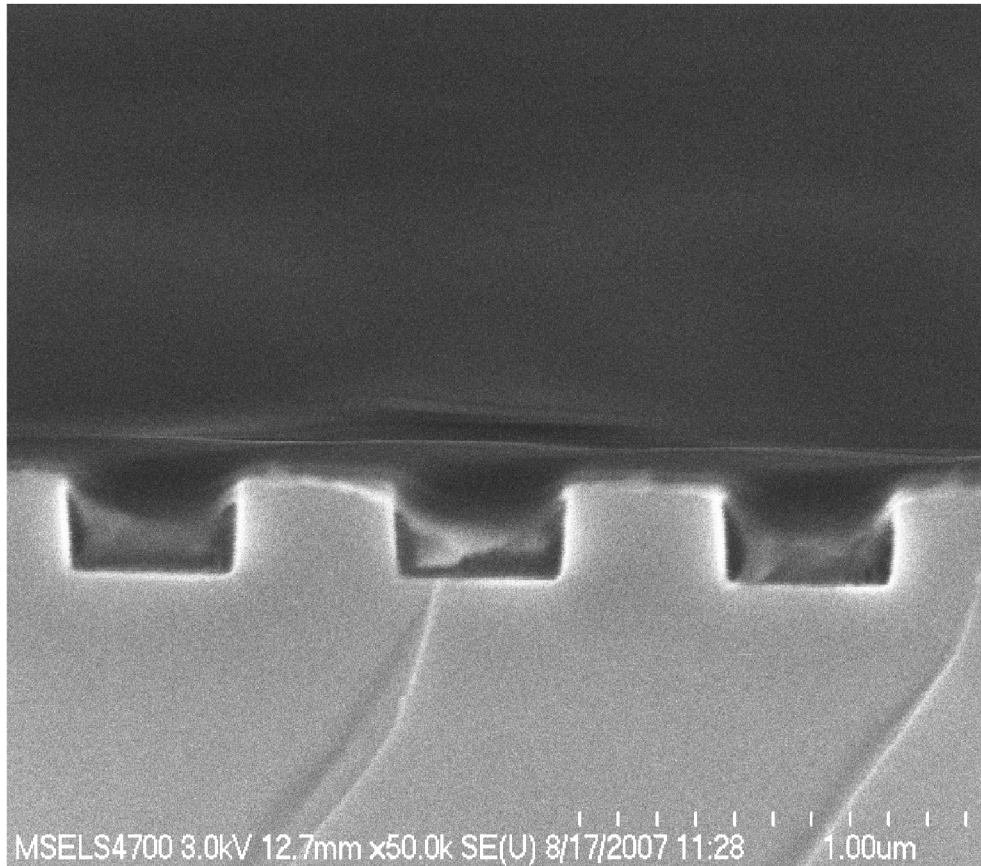


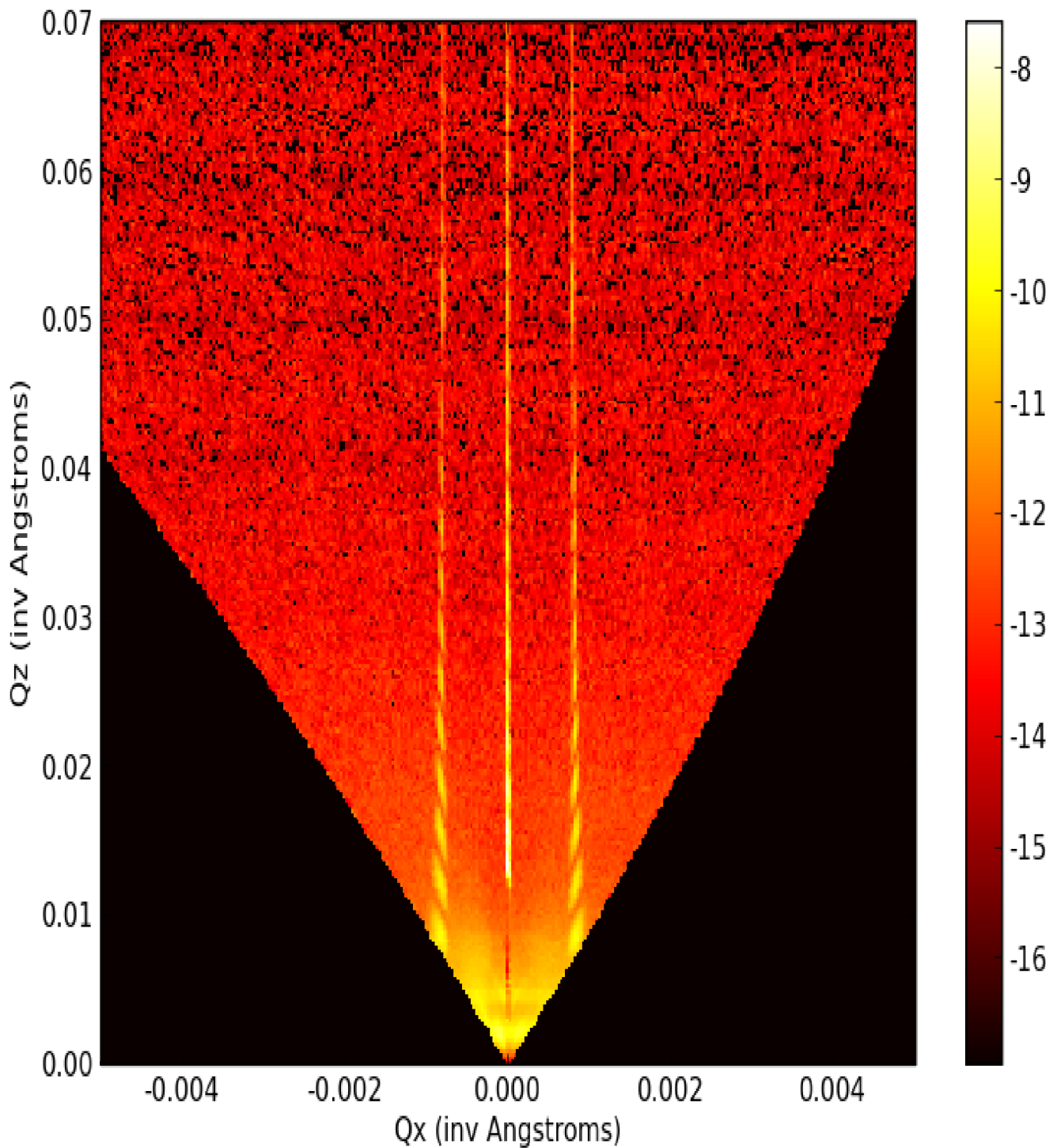
Illustration of the inverse relationship between the maximum value of  $Q$  up to which the reflectivity is measured and the spatial resolution in the corresponding SLD depth profile. Resolving smaller features in the profile in real space requires collecting reflectivity data up to larger values of  $Q$  in reciprocal space. The statistical accuracy in the measured reflectivity also affects the level of uncertainty in the associated SLD profile model to which the reflectivity data are fit.

# Diblock copolymer lamellar nanostructures –

R.Jones, B.Berry, and K.Yager (NIST Polymer Division) and  
S.Satija, J.Dura, B.Maranville et al. (NCNR).



Side-view scanning-electron micrograph of laser-interferometry-produced silicon substrate with 400 nm channels, spaced by 400 nm for a total repeat distance of 800 nm.



Neutron diffraction from silicon with channels cut in the surface in a periodic grating structure (as shown in the previous slide) without any material in the troughs. Using a position-sensitive-detector, both specular reflectivity (along the vertical  $Q_z$  axis) and non-specular (along the horizontal  $Q_x$  axis) can be collected.

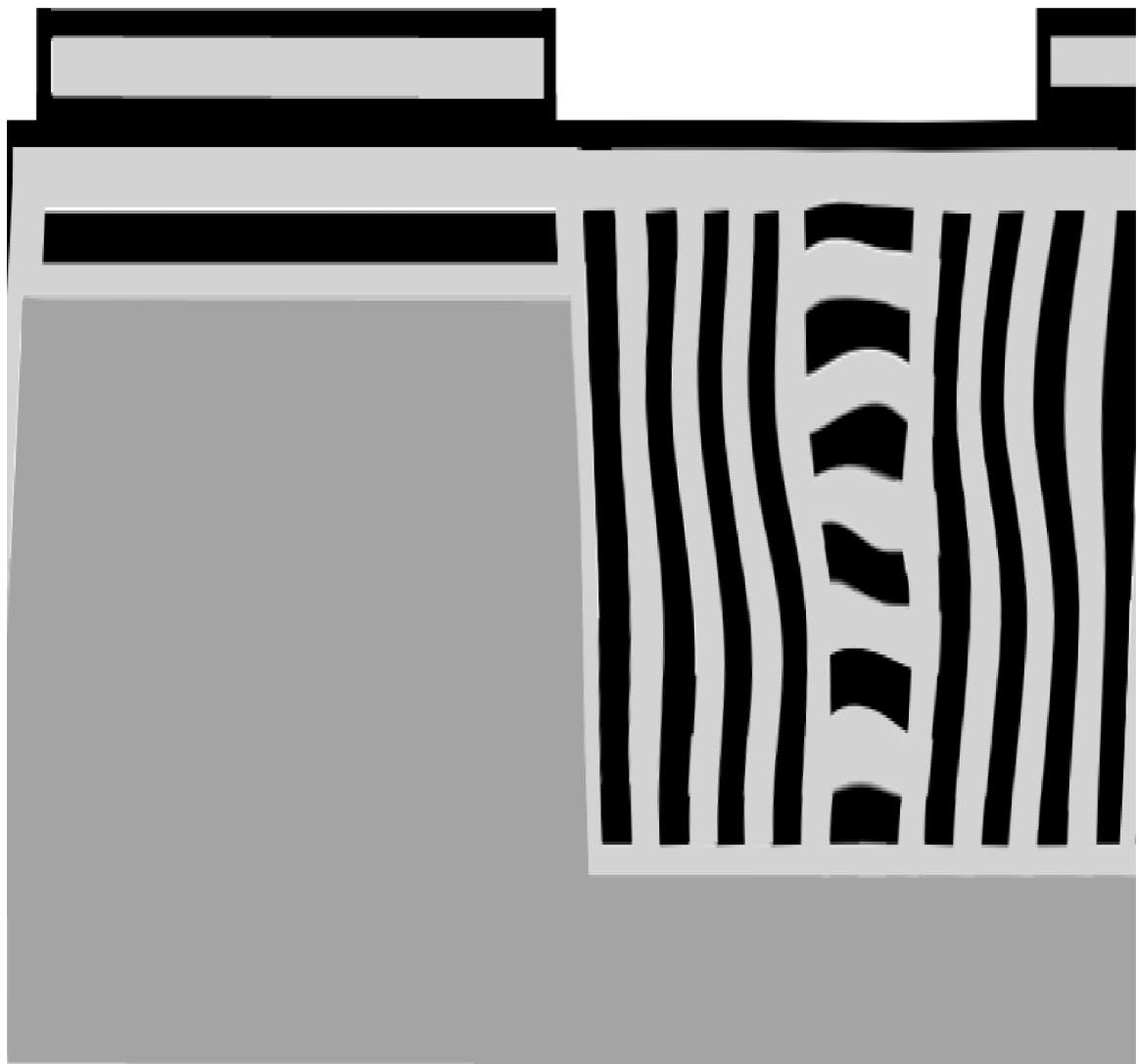
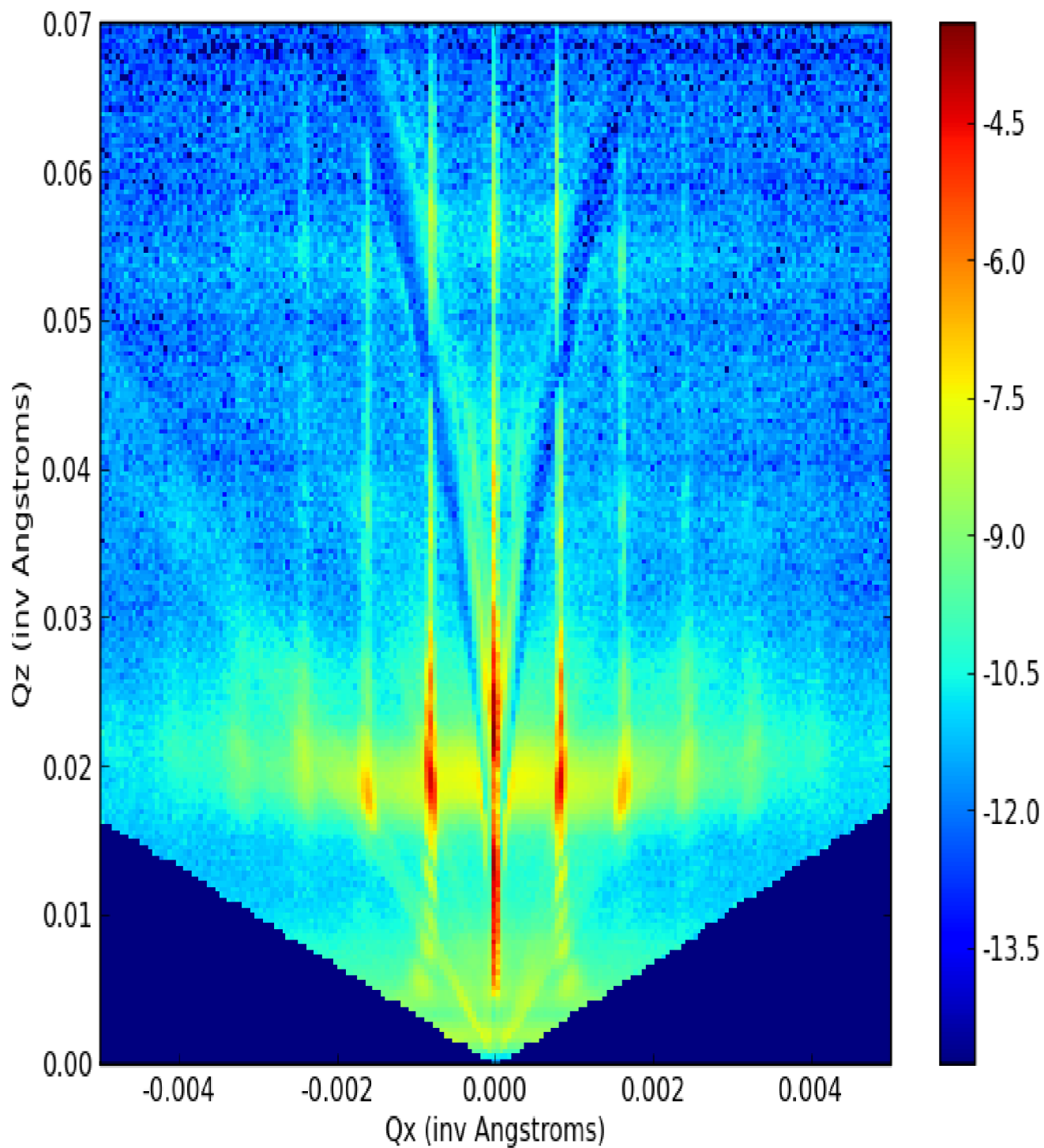
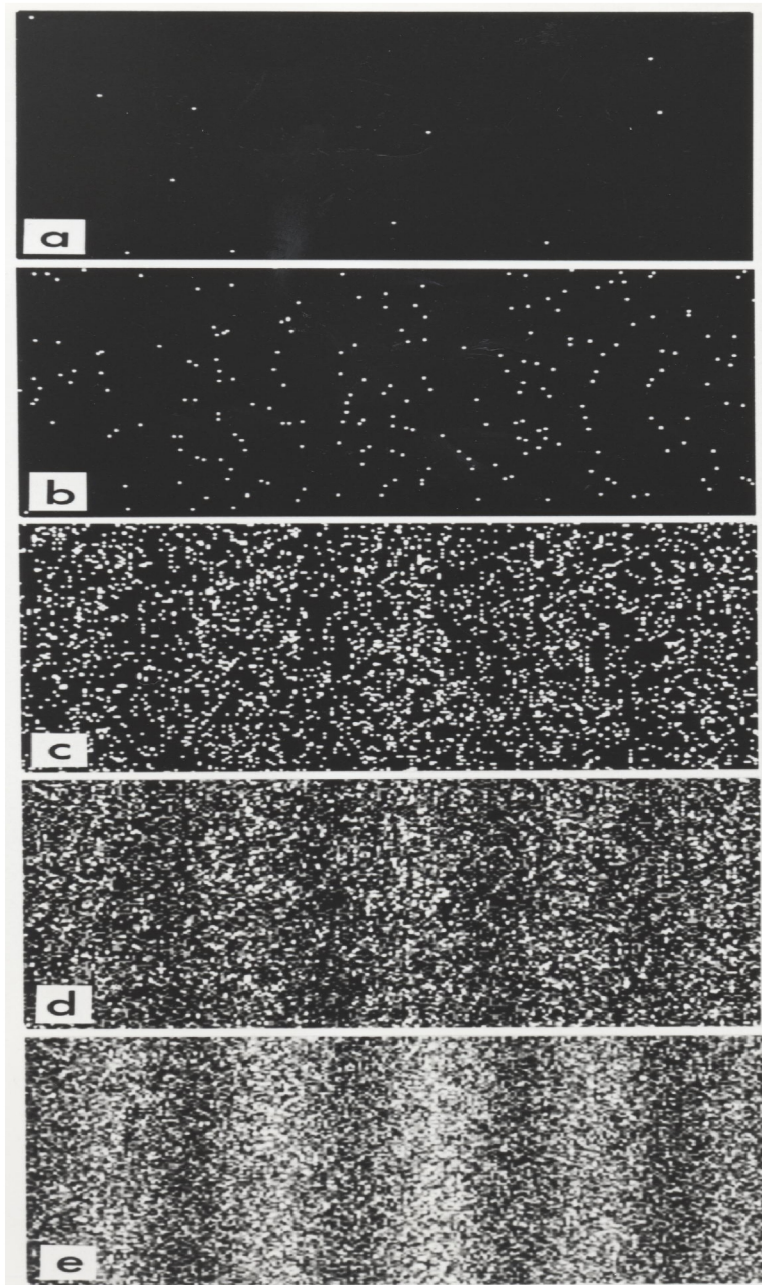


Diagram of expected orientation of di-block copolymer lamellae, with respect to the channels in the Si. The silicon substrate with etched channels is displayed in gray, with other lighter and darker regions corresponding to the two separate polymer components of the lamellae.



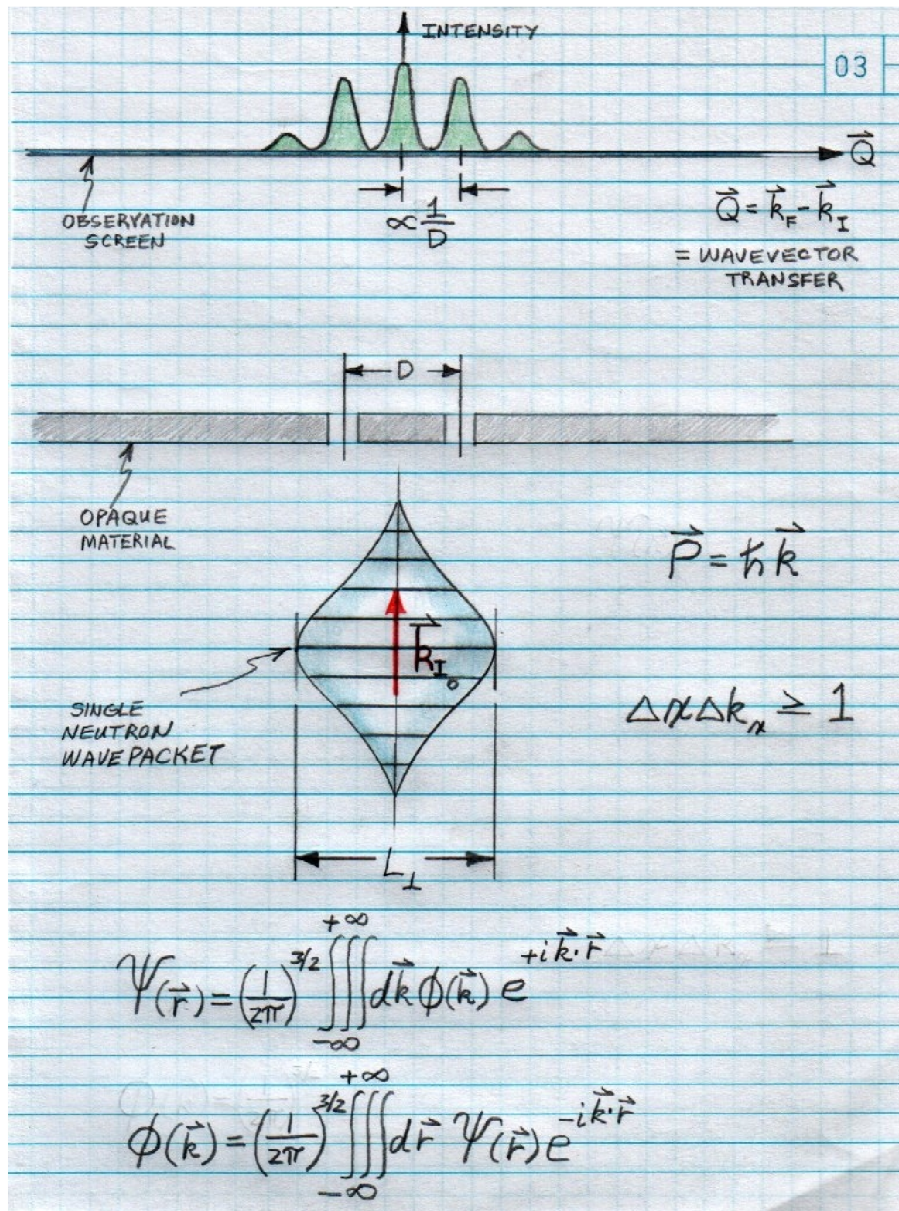
Neutron diffraction from Si channels filled with ordered di-block copolymer.

## Part 2: Neutron wave characteristics and coherence



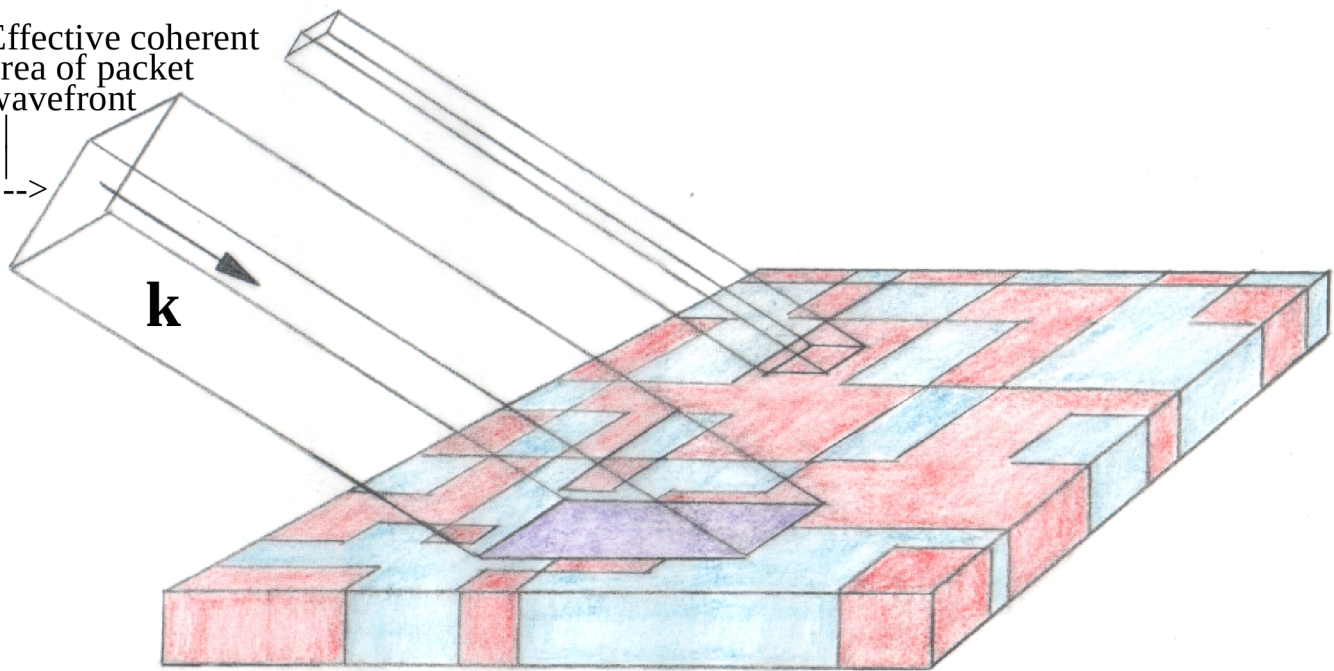
Electron diffraction pattern from a double slit -- one electron at a time (courtesy of Dr. Tanamura via Wikipedia.org). A liquid hydrogen moderator at a nuclear reactor facility acts as a spatially and temporally incoherent source of non-interacting, independent, individual neutrons described by wave packets which are to some degree localized in space. A collection of these individual wave packets can form a beam for use in a scattering instrument. The angular and energy distributions of the mean wave vectors associated with the neutron wave packets which make up a beam can be described as an incoherent instrumental resolution, as mentioned previously. (An incoherent source such as this is very different than a laser, for example, which produces photons in a highly-correlated, many-body state.)

Double slit diffraction of a wave packet describing a matter wave such as a neutron is depicted in the figure below.



Although the representation of a neutron as a plane wave is accurate as a solution of the one-dimensional Schroedinger wave equation for certain descriptions of specular reflection, there are important limitations. A plane wave is a mathematical idealization that has infinite spatial extent (and possesses, therefore, wavefronts which are perfectly coherent). This is physically unrealistic -- the neutron has a wave / particle duality and must be localized to some extent in space in a way that is consistent with the Heisenberg uncertainty relation of quantum mechanics. A single neutron interferes with the diffracting object by itself -- but the interference pattern becomes evident only after a sufficient number of such neutrons are collected at various locations in a detector to provide the required statistical accuracy.

Effective coherent area of packet wavefront



The effective transverse coherence area perpendicular to the propagation direction of the neutron wave packet is projected onto the film surface defining an area over which in-plane variations in SLD are averaged over in the specular process (note that the glancing angle of incidence enhances the projection along one in-plane direction):

$$r = (4\pi / (iQ)) \int_{-\infty}^{+\infty} \psi_{kz}(z) \langle \rho(x,y,z) \rangle_{x,y} e^{ikz} dz$$

$$\langle \rho(x,y,z) \rangle_{x,y} = (1/A) \int_{-\infty}^{+\infty} \rho(x,y,z) dx dy$$

The length scale of the SLD variations must be small enough for effective averaging to occur within the projected area. (The purple shaded area is meant to represent the coherent average of separate areas of “red” and “blue” SLD.) If not, then the net measured reflected intensity  $|r|^2$  is an area-weighted sum of reflectivities, each corresponding to an in-plane averaged SLD within a particular respective area, as depicted schematically in the figure above for the case of two distinct areas of different SLD (red and blue areas):

$$|r_{\text{NET MEASURED}}|^2 = (A_{\text{RED}} / A_{\text{TOTAL}}) |r_{\text{RED}}|^2 + (A_{\text{BLUE}} / A_{\text{TOTAL}}) |r_{\text{BLUE}}|^2$$

Figure 13

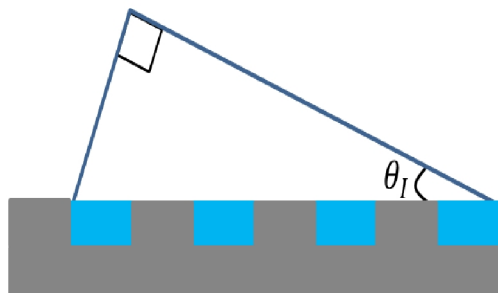
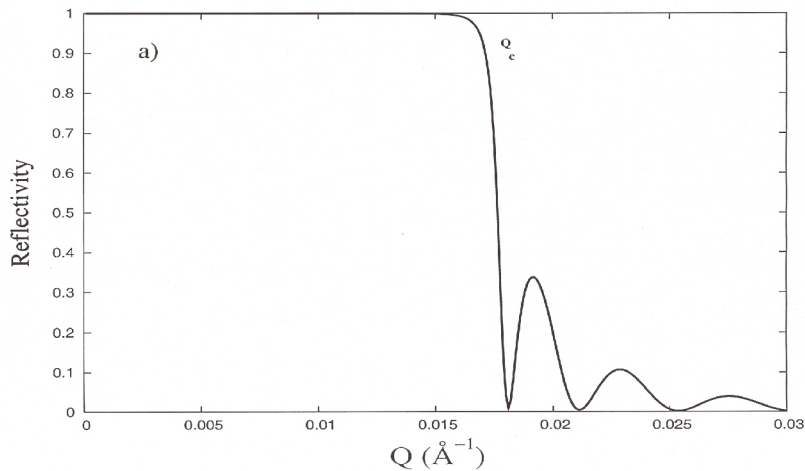
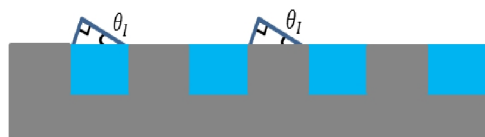
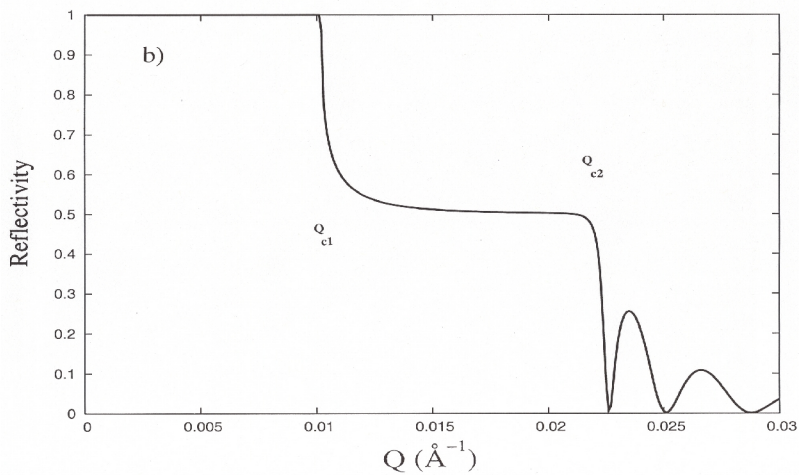
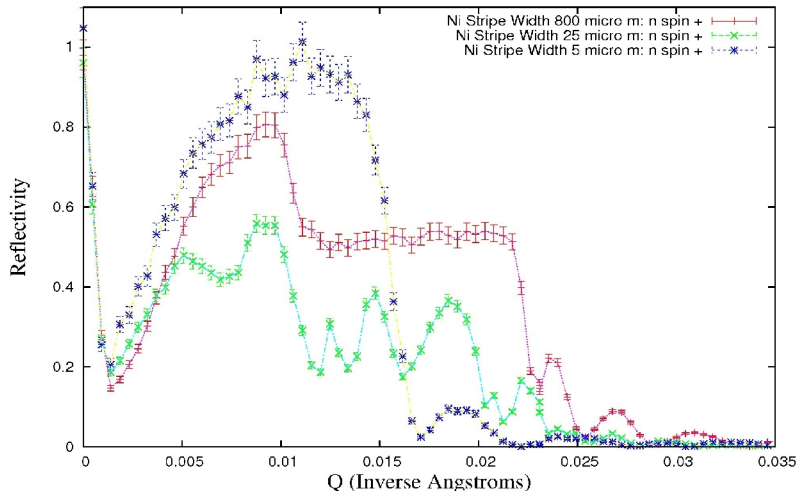


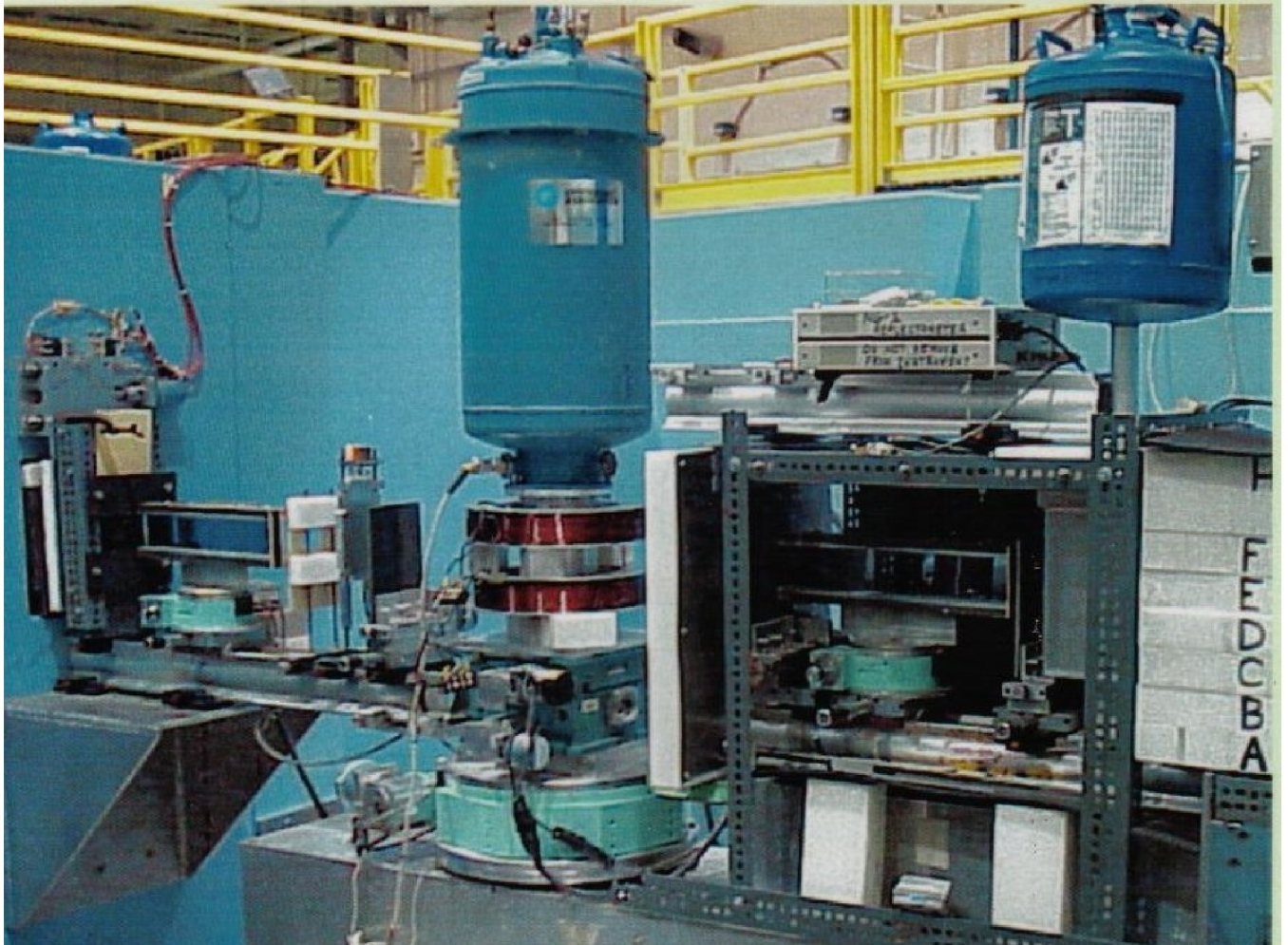
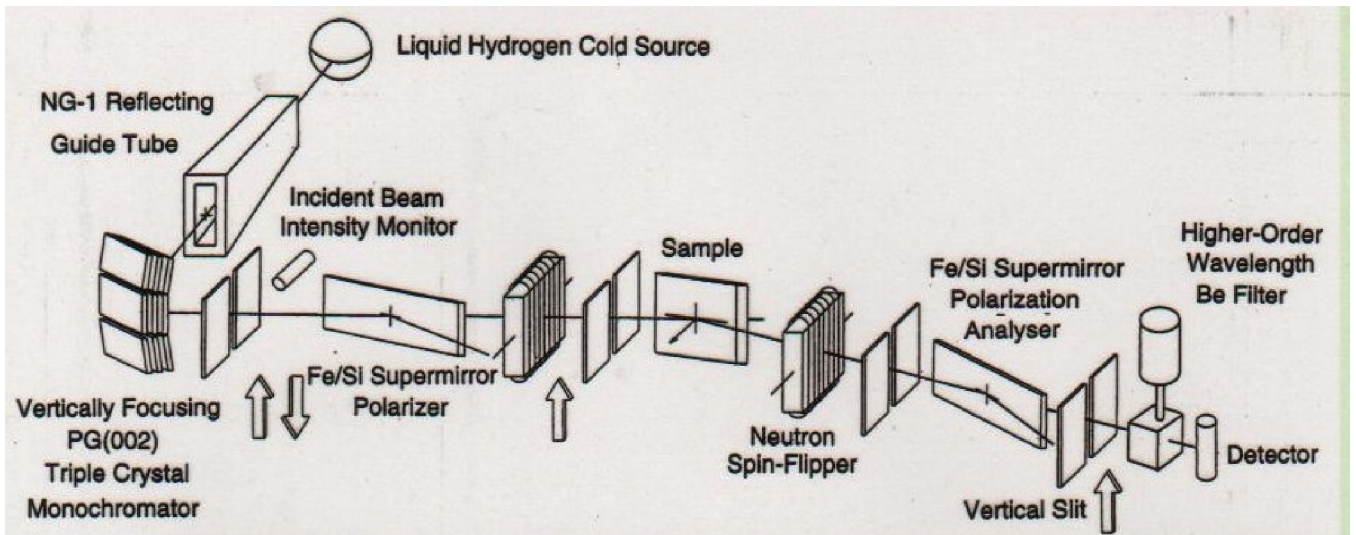
Figure 13



Model grating structures composed of two materials with different SLD values. Top -- the wave front of the neutron packet effectively averages over the in-plane density variations in specular reflection so that only a single critical angle is observed. Middle -- case where transverse coherence of the wavefront (perpendicular to the packet's mean  $\mathbf{k}$  vector) is not large enough to average so that two critical edges, one for each material SLD, are evident. Bottom -- actual neutron specular reflectivity data (without geometrical footprint correction) corresponding to examples for all three cases: coherent averaging; an incoherent sum of separate weighted reflectivities; and an intermediate case.

Grating Stripes Perpendicular to Scattering Plane





Polarized neutron reflectometer at NIST

## Neutron polarization -- fundamental concepts

<> a magnetic moment arises from the motion of electrical charges -- though neutral, a neutron is composed of charged quarks which give rise to a net magnetic dipole moment which is quantized with corresponding spin  $1/2$  -- a neutron is a Fermion

<> if it exists at all, any neutron electric dipole moment is of negligible magnitude for all practical purposes of concern to us here

<> a neutron can be represented by a spinor wave function having two components corresponding to two spin eigenstates (spin “+” or “up” and “-” or “down”)

<> for a nucleus with spin, the neutron-nucleus (i.e., the *nuclear*) interaction is spin-dependent

<> the *magnetic* interaction between the neutron magnetic moment and that of a *nuclear* magnetic moment is relatively weak (and nuclear magnetic moments are normally not ordered -- a notable exception occurring in a  $^3\text{He}$  gas cell used as a neutron polarizer)

<> the *magnetic* interaction between the neutron magnetic moment and that of an atomic magnetic moment, on the other hand, can be comparable to the nuclear interaction

(a good description of the phenomenon of a quantized spin one-half system is given in the quantum mechanics text by Merzbacher)

$$\Psi = \psi_+ + \psi_- = \underbrace{C_+ e^{i\vec{k}_+ \cdot \vec{r}}}_{C_+} \begin{pmatrix} 1 \\ 0 \end{pmatrix} + \underbrace{C_- e^{i\vec{k}_- \cdot \vec{r}}}_{C_-} \begin{pmatrix} 0 \\ 1 \end{pmatrix}$$

$$k_{\pm} = m_{\pm} k_0$$

$$m_{\pm}^2 = 1 - \frac{2m}{(\hbar k_0)^2} (V_N \pm \mu B)$$

$$= 1 - \frac{4\pi}{k_0^2} (\rho_N \pm \rho_M)$$

NUCLEAR  
SLD

MAGNETIC  
SLD

---


$$|\Psi|^2 = \Psi^{*T} \Psi = (\psi_+^* \psi_-^*) \begin{pmatrix} \psi_+ \\ \psi_- \end{pmatrix}$$

$$= \psi_+^* \psi_+ + \psi_-^* \psi_-$$

$$= C_+^* e^{-i\vec{k}_+ \cdot \vec{r}} C_+ e^{+i\vec{k}_+ \cdot \vec{r}} + C_-^* e^{-i\vec{k}_- \cdot \vec{r}} C_- e^{+i\vec{k}_- \cdot \vec{r}}$$

$$= |C_+|^2 + |C_-|^2 = 1$$

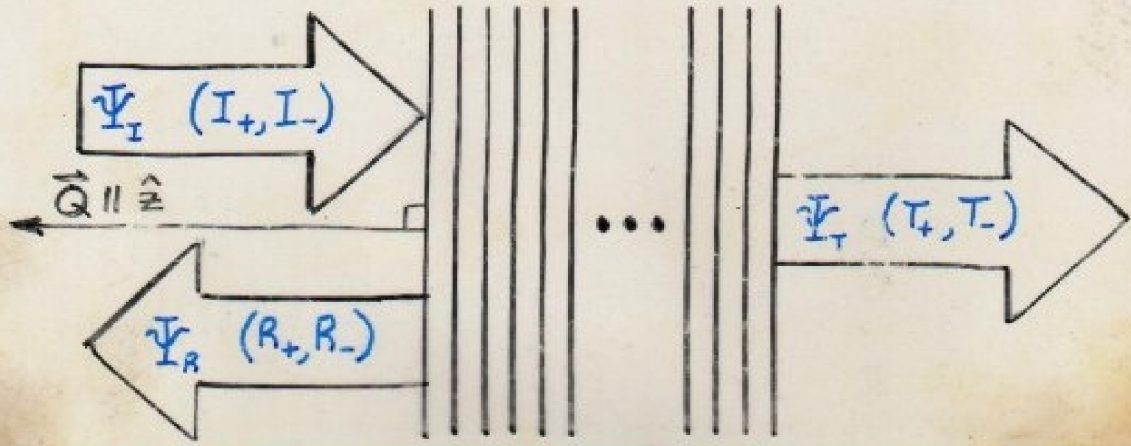
The neutron is a spin-half quantum object and possesses a corresponding magnetic moment. Its wave function must therefore be described as a “spinor” which is composed of two terms, each representing one of two possible spin “eigenstates”. In a magnetic field, the energies associated these two eigenstates are different. This can have significant consequences for the interaction of the neutron with magnetic fields and materials.

So our description of a neutron gets a bit more complicated when we have to take into account its spin and moment. But, as I hope you will see, that added complexity makes the neutron a more sensitive and useful probe of matter, even that which is not itself magnetic.

The magnetic SLD is a product of the number of magnetic atoms per unit volume times their characteristic magnetic scattering length (usually designated “p”) -- or is proportional to a macroscopic magnetic induction field “B”.

GENERAL MULTILAYER REFLECTIVITY  
CALCULATION FOR POLARIZED NEUTRONS

$$\left[ \frac{-\hbar^2}{2m} \nabla^2 + (V-E) \right] \Psi = 0 \quad \Psi = \begin{pmatrix} \Psi_+ \\ \Psi_- \end{pmatrix}$$



$$V_N = Nb$$

$$V_M = -\vec{\mu} \cdot \vec{B}$$

$$\frac{\partial^2}{\partial z^2} \Psi_+ + \left( \frac{Q^2}{4} - 4\pi\rho_{11} \right) \Psi_+ - 4\pi\rho_{12} \Psi_- = 0$$

$$\frac{\partial^2}{\partial z^2} \Psi_- + \left( \frac{Q^2}{4} - 4\pi\rho_{22} \right) \Psi_- - 4\pi\rho_{21} \Psi_+ = 0$$

$$\rho_{11} = Nb + Np \sin\theta \sin\phi$$

(22)                      (-)

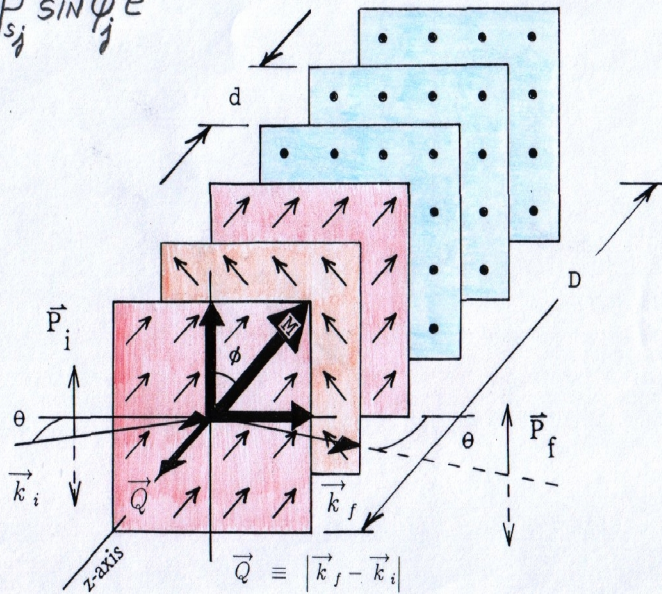
$$\rho_{12} = Np (\cos\theta - i \sin\theta \cos\phi)$$

(21)                      (+)

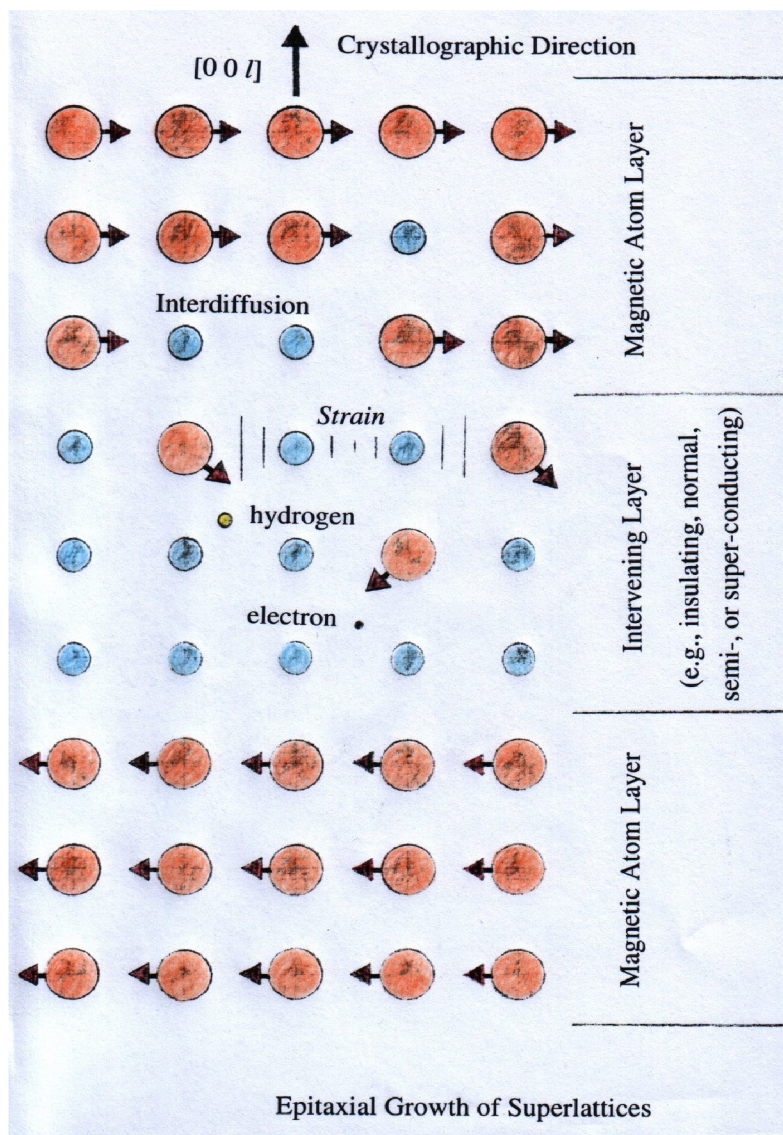
For polarized neutrons, solving the Schroedinger equation of motion -- say for specular reflection, as we have done previously in the absence of magnetic fields -- now requires a simultaneous solution of a pair of coupled equations. This takes into account the possibility that a scattering event or interaction will involve a change in the neutron's spin eigenstate from "+" or "up" to "-" or "down" (or not). Note that the nuclear and magnetic SLDs or potentials are additive and thus result in an interference in some cases that is neutron spin-dependent.

$$F^{\pm\pm} \propto \sum_{j=1}^N [b_{sj} \pm p_{sj} \cos \phi_j] e^{iQ_{uj}}$$

$$F^{\pm\mp} \propto \sum_{j=1}^N p_{sj} \sin \phi_j e^{iQ_{uj}}$$



The above diagram illustrates a particularly useful configuration resulting in the ability to determine not only the magnitude of the net magnetization in each of the successive planes in a layered material, but also the direction of that magnetic moment.

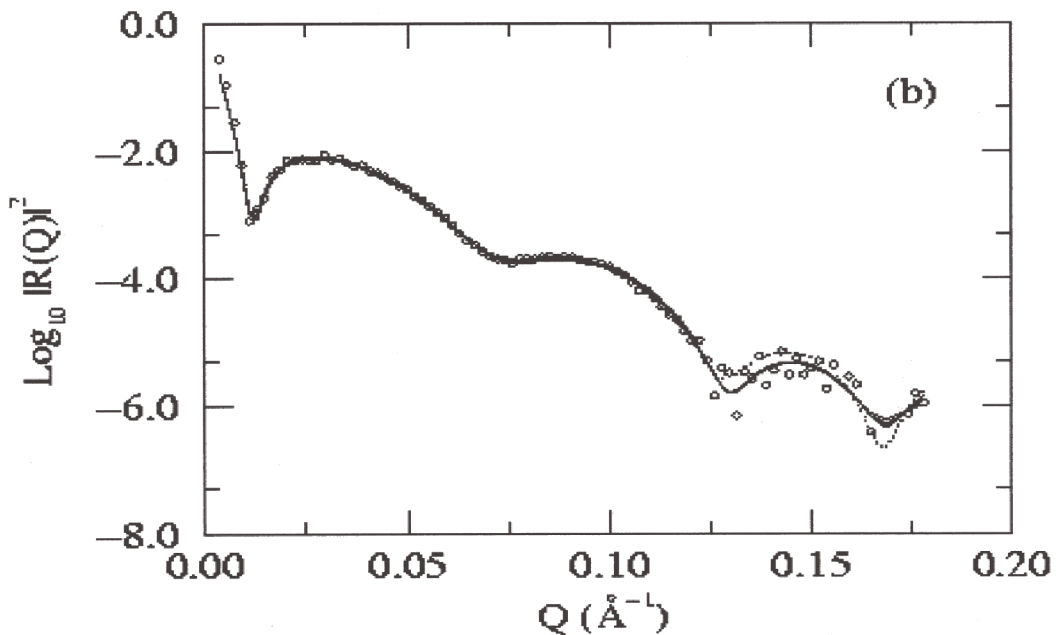
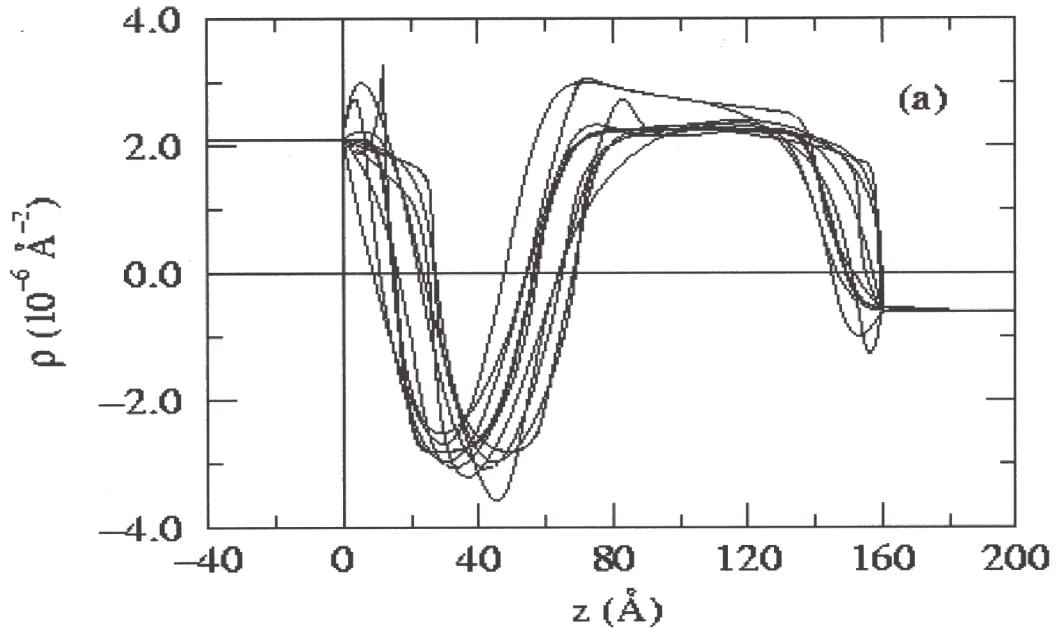


By means of molecular beam epitaxial growth in ultrahigh vacuum and other thin film deposition techniques, it is possible to construct synthetically layered systems tailored to study specific types of inter-actions of interest in hard condensed matter. For instance, how two separated regions made up of ferromagnetic atomic planes interact with one another across an intervening region of atomic planes of a material that is superconducting or semi-conducting can be studied by analysis of the polarized neutron reflectivity -- as a function of temperature, applied magnetic field magnitude and direction, or other parameter such as the thickness of the intervening layer.

There exists a considerable body of work on systems prepared in this manner.

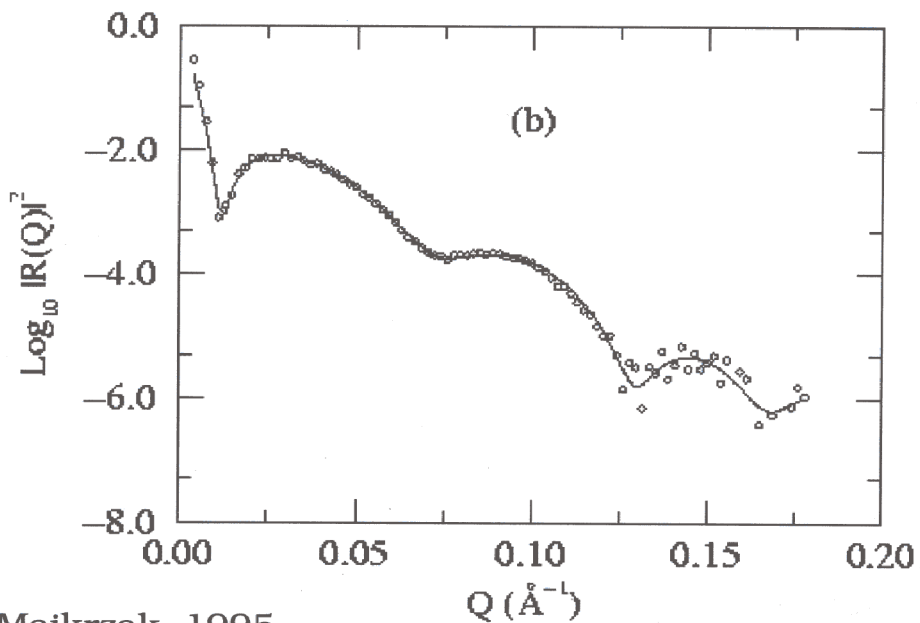
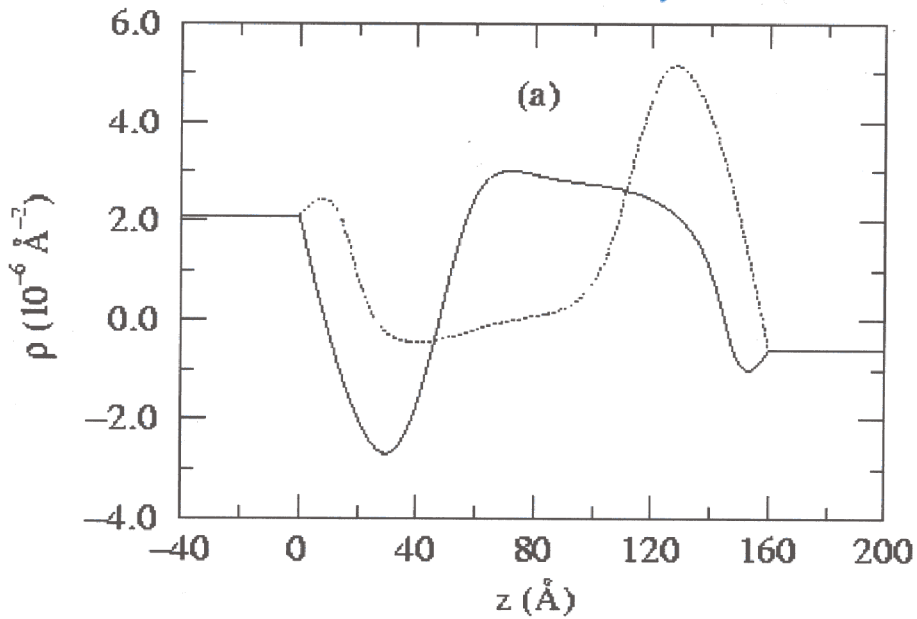
## Part 3: The Phase problem, Direct Inversion and Simultaneous Fitting

- <> ambiguous SLD profiles from reflected *intensities*
- <> measurement of reflection *amplitude* via references yields unique solution -- one-to-one correspondence with SLD profile
- <> given the reflection amplitude, exact, first-principles inversion to obtain unique SLD profile for specular reflection is possible
- <> simultaneous fitting of multiple composite (sample + reference) reflectivity data sets can lead to unambiguous solution as well



Repeated fits of reflectivity data from a Ti/TiO film system on a Si substrate in contact with an aqueous reservoir (Berk et al.). The variation among the individual fits is indicative of the accuracy attainable in the SLD profile given the truncation of the reflectivity data at a maximum value of  $Q$  and the statistical uncertainty in the data points.

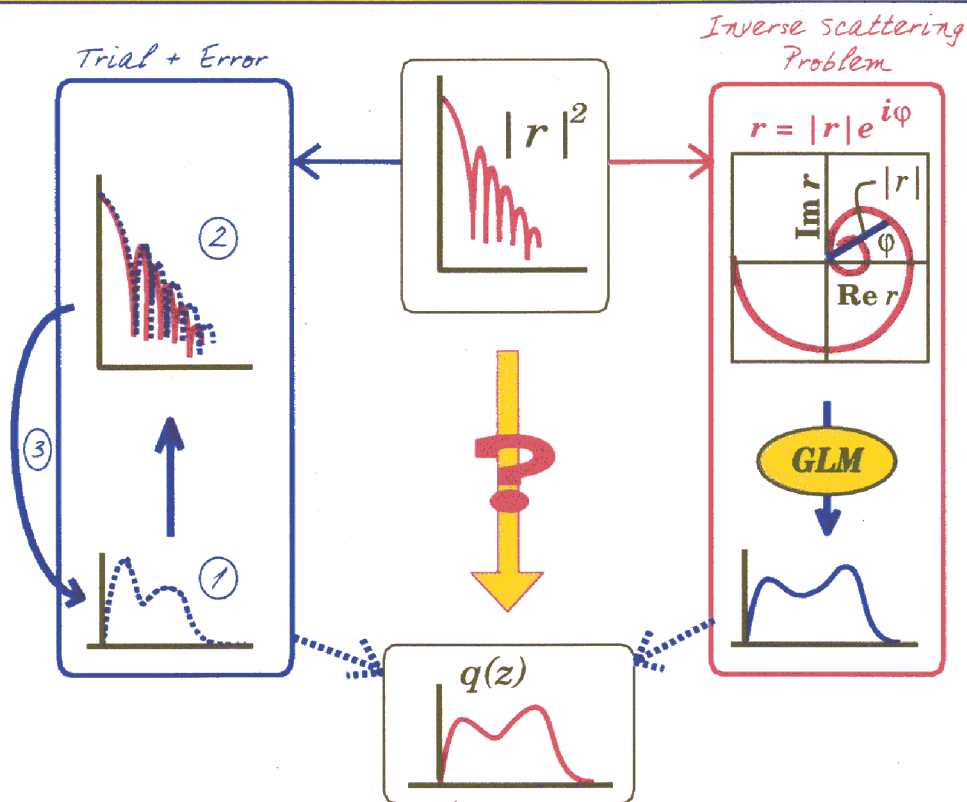
*TiO in situ: Wiesler, et al.*



Berk & Majkrzak, 1995

It was found that if enough individual fits were performed, another “family” of fits emerged (only one of which is shown above in comparison to a representative fit of the other family shown on the previous slide) with essentially the same chi-squared goodness of fit criteria -- this alternative SLD profile is a consequence of the loss of phase information inherent when the reflectivity  $|r|^2$  (proportional to the reflected *intensity*) is measured rather than the complex reflection *amplitude*  $r$  -- i.e., the non uniqueness arises from a loss of the phase information carried by the reflected wave function.

# Inverting reflectivity



## Phase determination

C.F. Majkrzak and N.F. Berk, Phys. Rev. B **52**, 10827 (1995).

V.-O. de Haan, et al., Phys. Rev. B **52**, 10830 (1995).

H. Leeb, H.R. Lipperheide and G. Reiss, this conference.

## Logarithmic dispersion

W.L. Clinton, Phys. Rev. B **48**, 1 (1993).

## Tunneling times

H. Fiedeldey, H.R. Lipperheide, et al., Phys. Lett. A **170**, 347 (1992).

## Pseudo-inversion

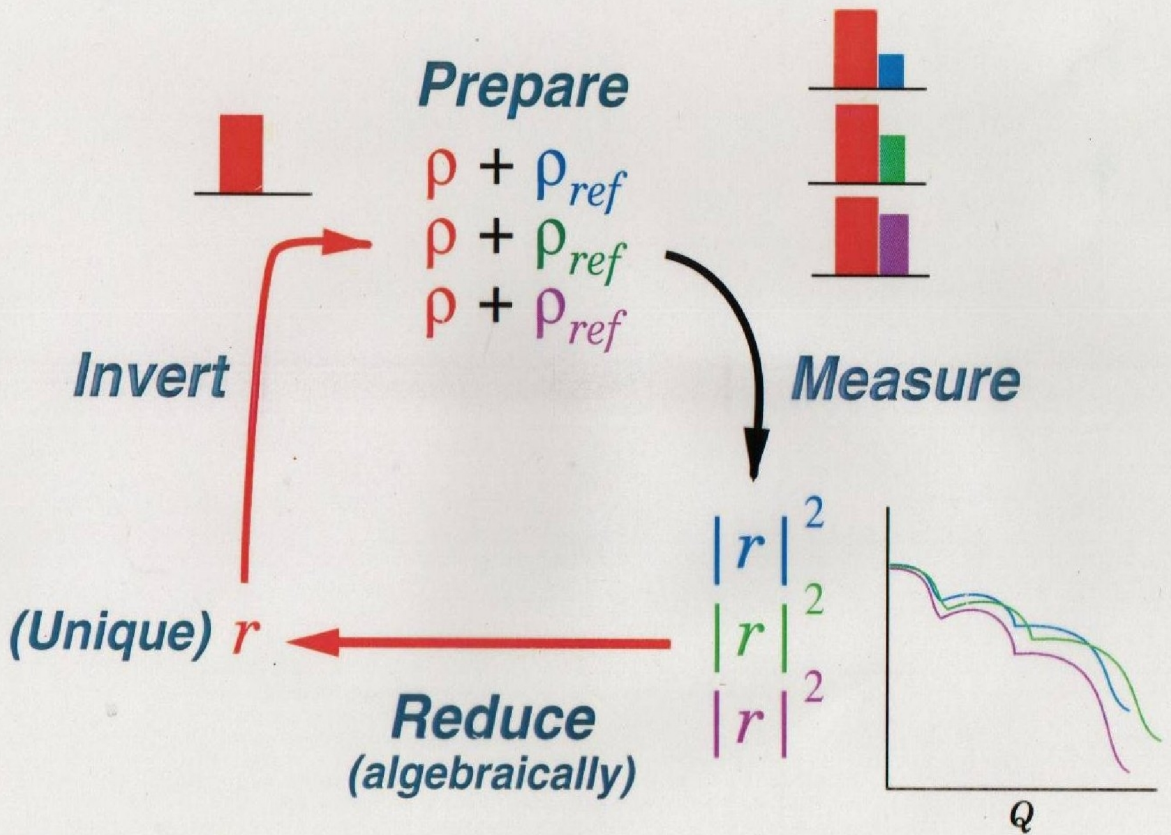
S.K. Sinha, et al., *Surface X-Ray and Neutron Scattering*, 85 (Springer, 1992).

C.F. Majkrzak, N.F. Berk, et al., SPIE Proc. **1738**, 282 (1992).

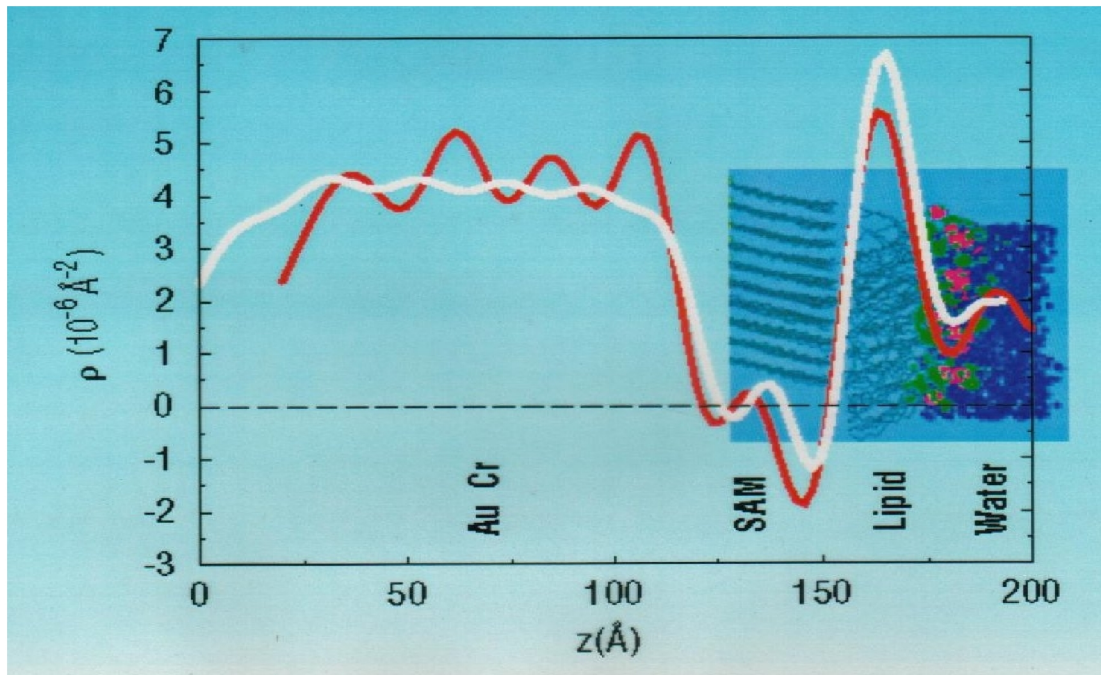
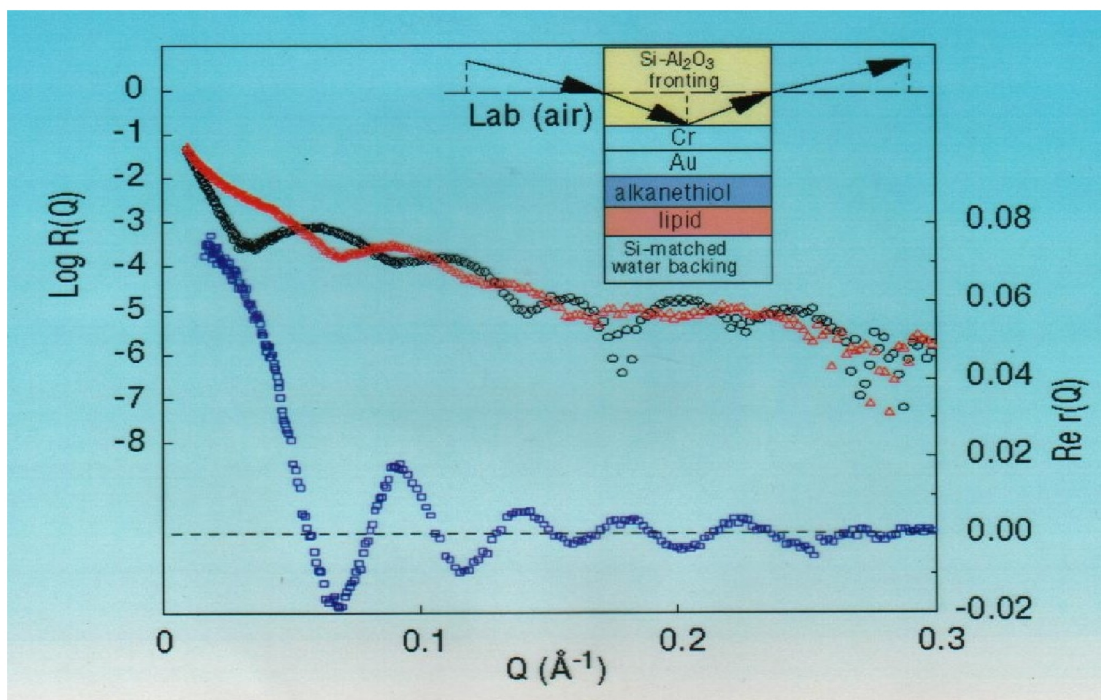
NIST

It turns out that it is possible to solve the phase problem for specular neutron reflectometry, in most cases, exactly, through the use of reference film layers -- in essence this is analogous to an interferometric method such as holography.

# Phase Determination with 3 References



Majkrzak & Berk, 1995  
de Haan, et al., 1995



In the upper figure, the red and black reflectivity curves correspond to two composite system reflectivity data sets for the film structure in the inset and either Si or  $\text{Al}_2\text{O}_3$  fronting medium -- from which the blue curve representing the real part of the reflection *amplitude* associated with the film structure of interest was obtained (here, the variable fronting media serve as the reference parts of the composite systems). In the lower figure is the SLD profile (in red) obtained from a first-principles inversion of the exact  $\text{Re } r$  (from the upper figure) -- the “ringing” evident in the gold layer region is due to a truncation of the reflectivity data at a finite  $Q$  maximum. The white curve is the SLD profile calculated by a molecular dynamics model simulation of the lipid bilayer membrane which was actually deposited on the substrate for the experiment.

## **Part 4: Applications of NR to studies of the nano-scale structure of thin film materials**

<> Soft condensed matter:

- polymers

- bio-membranes

- organic photo-voltaic films

...

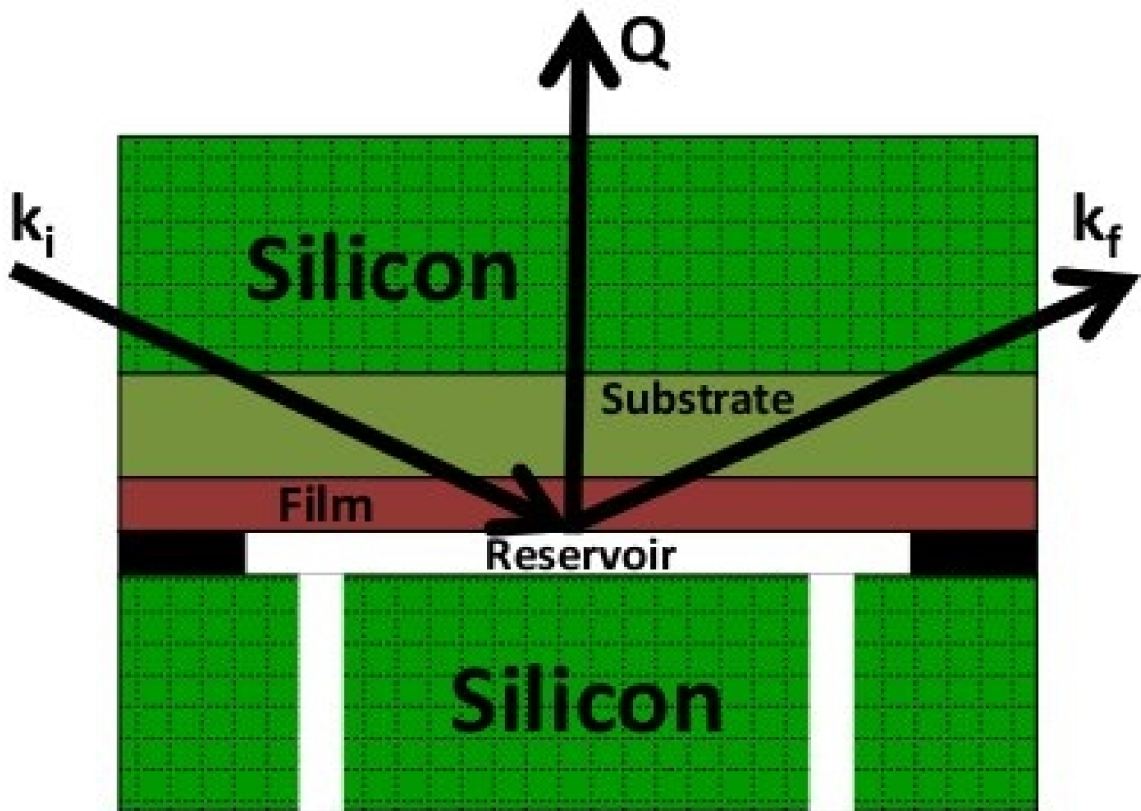
<> Hard condensed matter:

- magnetic materials (to be discussed in a following lecture)

- chemical interdiffusion (e.g.,  $^{58}\text{Ni}/^{62}\text{Ni}$ )

- metal hydrides

...



Fortunately, neutrons can be transmitted through macroscopic thicknesses of single crystal materials such as Si -- consequently, it is possible to construct fluid cells in which a deposited thin film structure of interest can be placed adjacent to an aqueous reservoir, for instance. Experiments can then be conducted as a function of PH, salinity, temperature, flow, etc., in-situ.

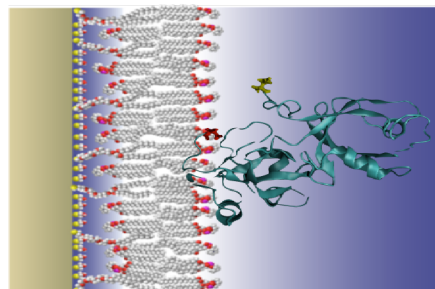
A sampling (on this and the next slide) of more recent specular NR studies of compositional depth profiles of biological macromolecules attached to or embedded in lipid bilayer membranes. These results are remarkable -- if not spectacular (at least in my opinion)!

## Water-soluble membrane-associated proteins

>50% of biological NR beam time for biomedical applications using tBLMs

### Active projects (last 2 cycles):

- Dengue
- Gaucher's disease
- GRASP
- HIV Gag & antibodies
- RSV & MLV
- Neurotransmitter
- OmpA/LA
- Parkinson's disease
- PTEN Tumor suppressor
- T-Cell receptor



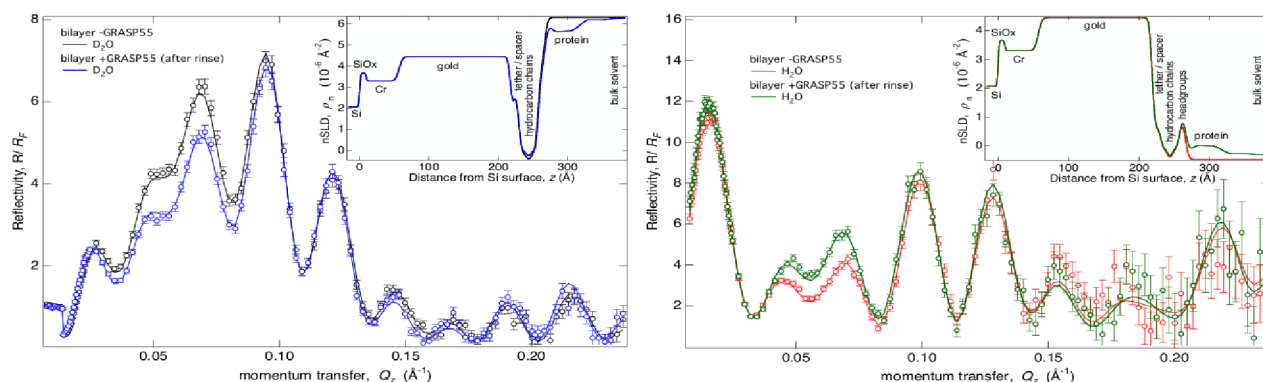
GRASP orientation at a tethered bilayer lipid membrane (tBLM) as determined by NR

### Collaborative staff involvement:

- experimental planning
- substrate preparation
- tether synthesis
- neutron measurement
- data analysis

Bulent Akgun, Frank Heinrich, Mathias Lösche, Duncan McGillivray, Hirsh Nanda, David Vanderah

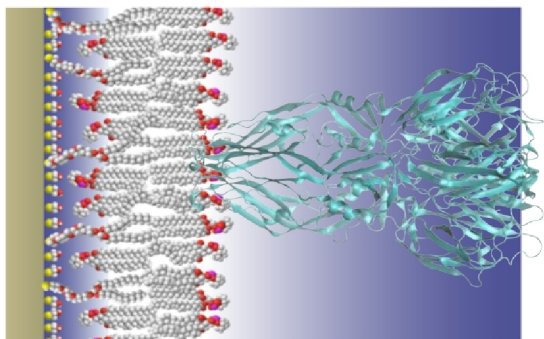
## Typical reflectometry data for tBLM experiments



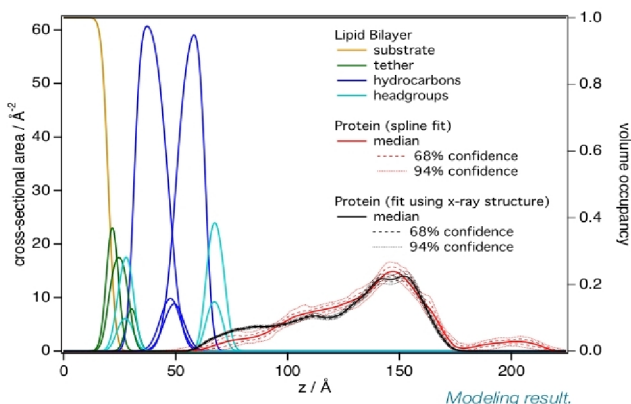
NR data measured on NG7, and best-fits for GRASP association with lipid membranes, project with A. Linstedt, University of Pittsburgh

Bulent Akgun, Frank Heinrich, Mathias Lösche, Duncan McGillivray, Hirsh Nanda

# Example: Dengue Virus Envelope Protein



Visualization. Project with Mike Kent, Sandia National Labs.



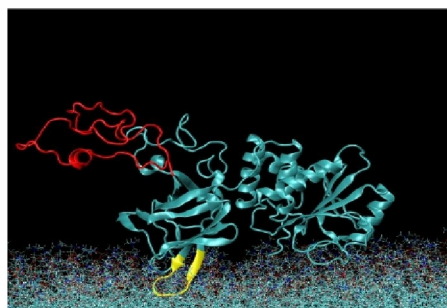
- Monte-Carlo Markov Chain uncertainty analysis
- Composition-space modeling of the bilayer
- Free-form fitting of structurally unknown components of the architecture
- Usage of PDB structure files for position and orientation of rigid proteins

Bulent Akgun, Frank Heinrich, Paul Kienzle, Sushil Satija

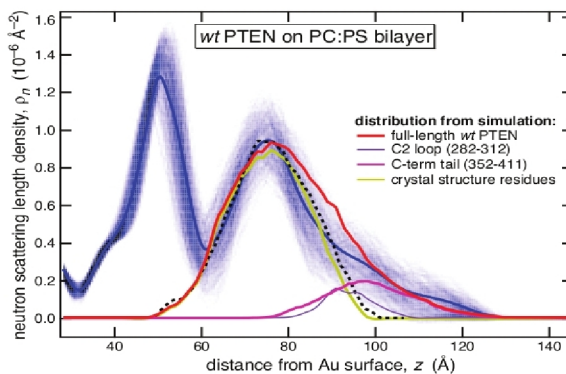


[www.ncnr.nist.gov/programs/reflect/](http://www.ncnr.nist.gov/programs/reflect/)

# Combining NR with Molecular Simulations



MD simulation snapshot of PTEN tumor suppressor association with a PS-containing lipid membrane



Comparison of experimental data with results from:

- MD simulation
- Monte Carlo conformational search (SASSIE) results

Future Challenges:

- Ensemble averaging, integrating NR and simulation

Joseph Curtis, Mathias Lösche, Hirsh Nanda



# Nanoparticle distribution in polymer-based solar cells affects solar cell performance: A neutron reflectivity study

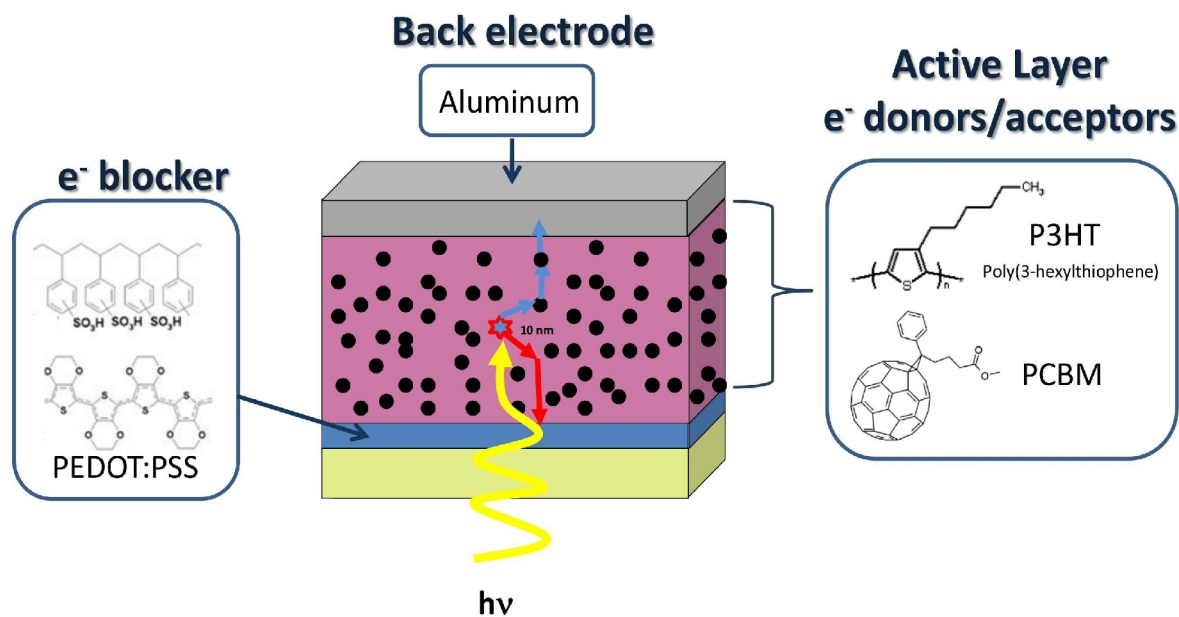
Jonathan Kiel<sup>1</sup>, Brian Kirby<sup>2</sup>, Charles Majkrzak<sup>2</sup>,  
Brian Maranville<sup>2</sup>, Michael Mackay<sup>3</sup>

Thursday, August 20th, 2009

- 1) Michigan State University, Department of Chemical Engineering and Materials Science
- 2) National Institute of Standards and Technology, Center for Neutron Research
- 3) University of Delaware, Materials Science and Engineering



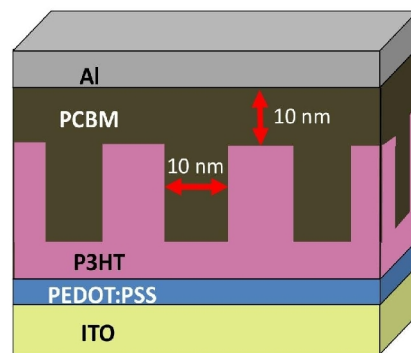
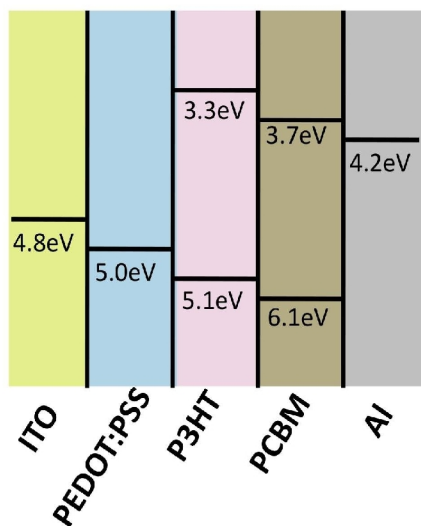
# Components of organic solar cells



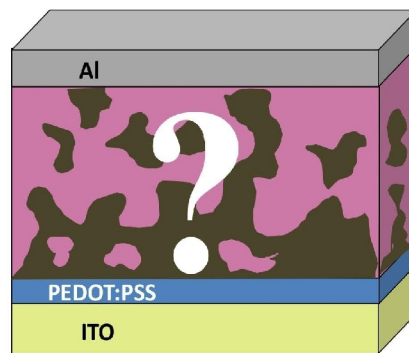
- Exciton diffusion length  $\sim 10$  nm
- PCBM:P3HT morphology very important

# What is the morphology of the active layer

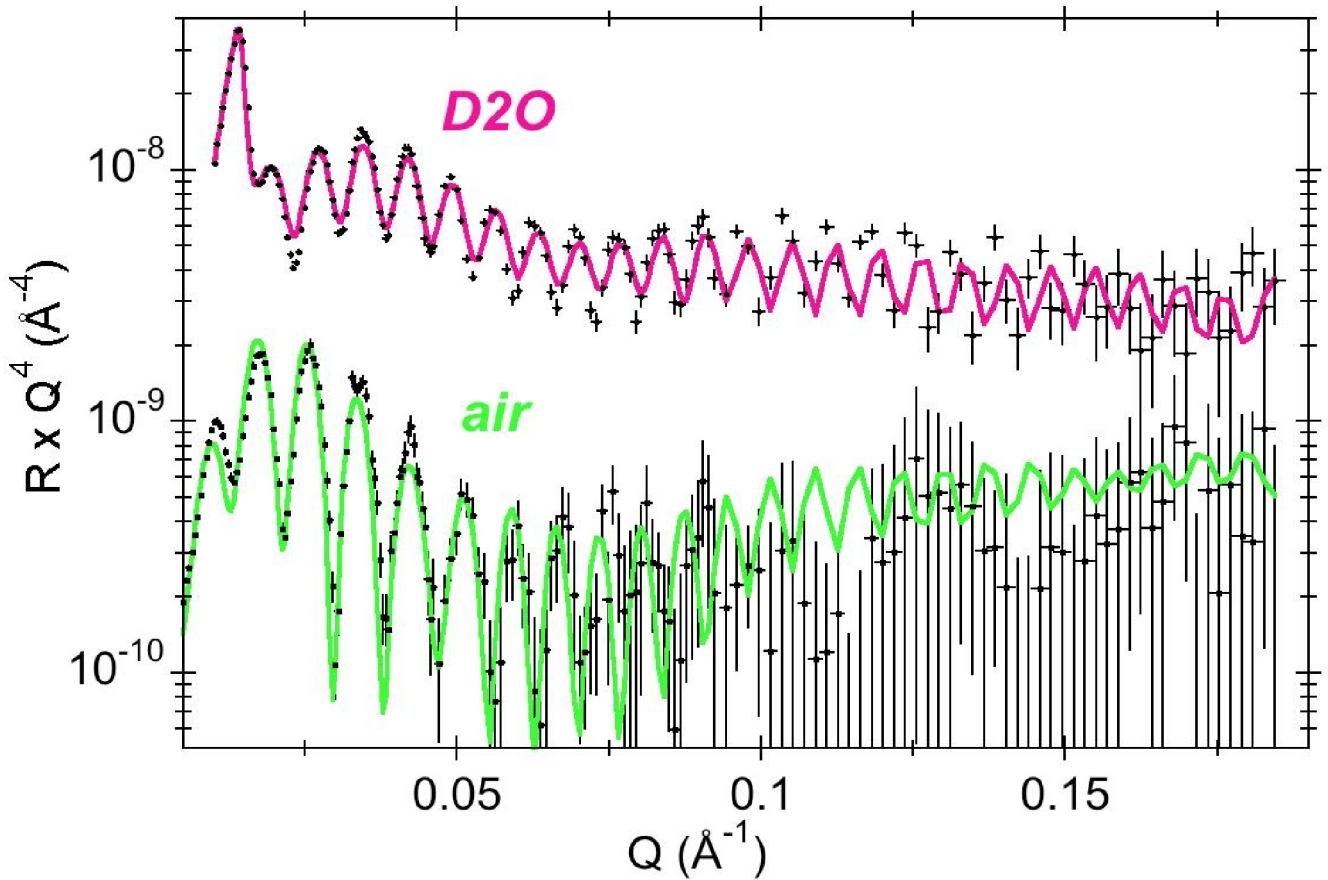
Energy Diagram of Organic Solar Cell



Idealized morphology

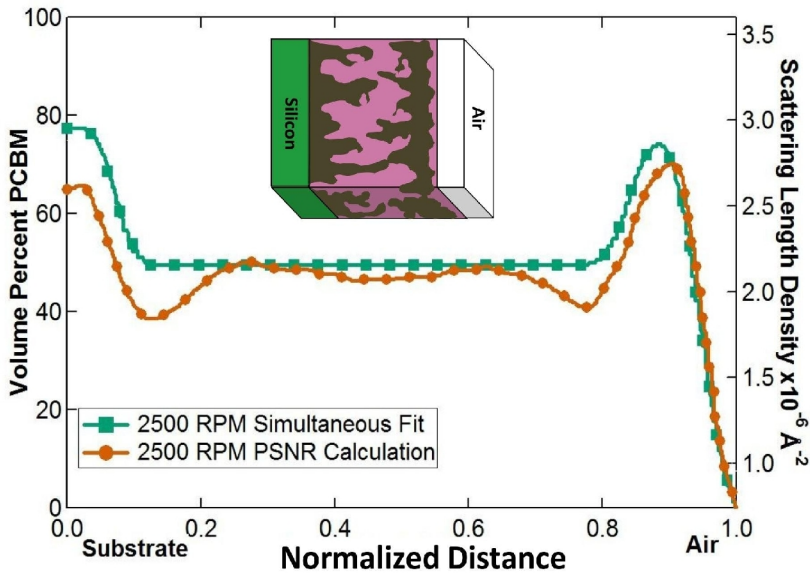


Actual morphology



Reflectivity data collected from the same film system with two different backing media -- air and deuterated water. Once again, the reason for collecting such composite system (reference plus unknown part) reflectivity data is to be able to retrieve the phase information.

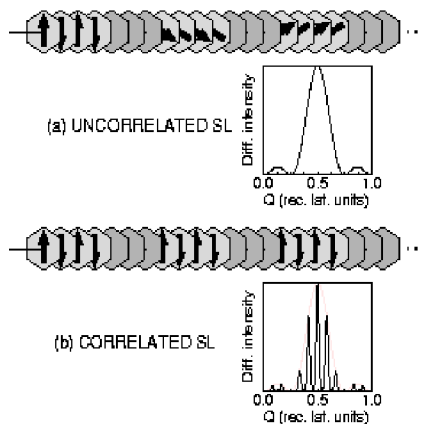
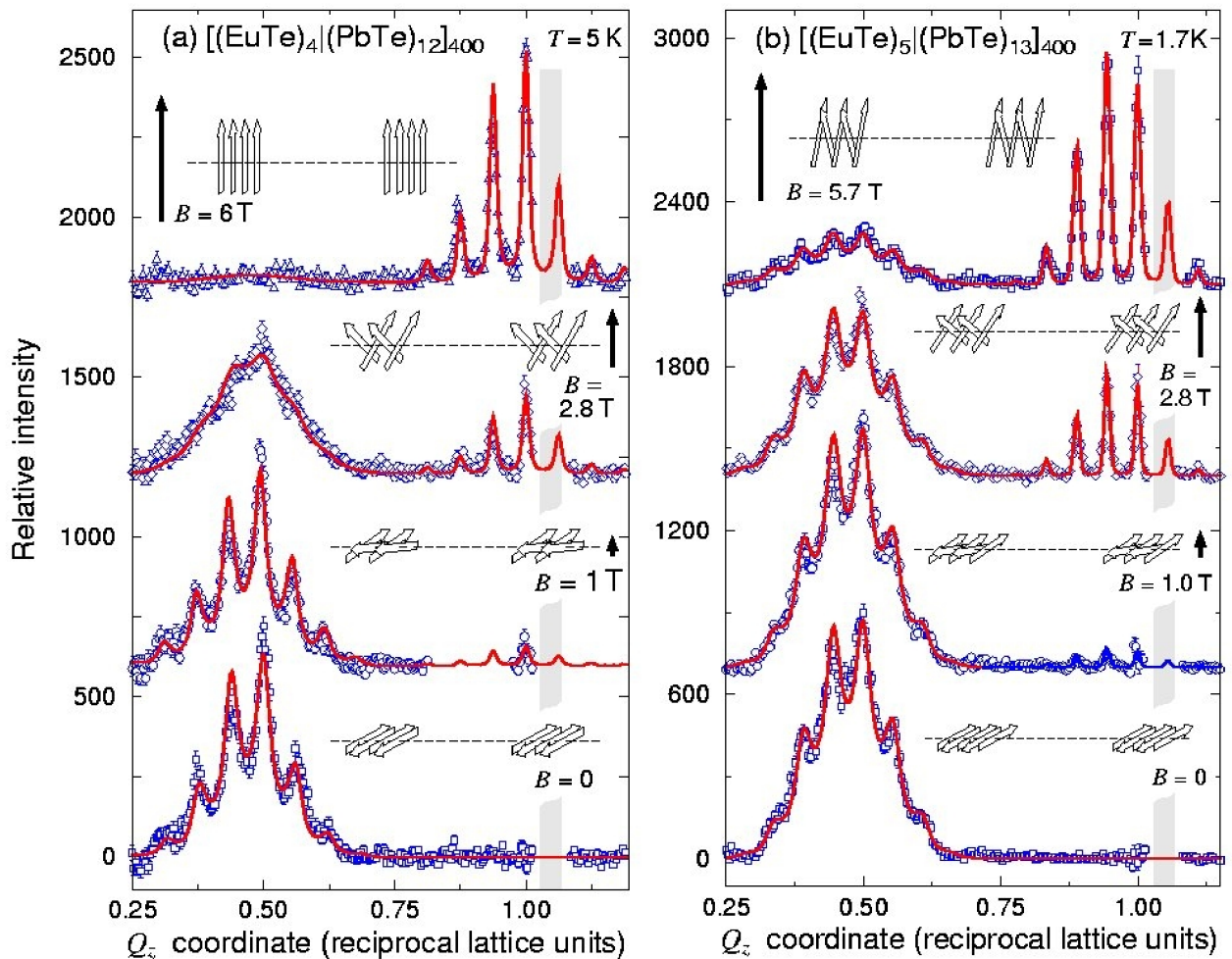
# PCBM Volume % Comparison



- Simultaneous fitting and PSNR calculations show great agreement
- High PCBM concentration at substrate
- High PCBM concentration near air interface

$$\text{Vol\% PCBM} = \frac{\text{SLD}_{\text{measured}} - \text{SLD}_{\text{P3HT}}}{\text{SLD}_{\text{PCBM}} - \text{SLD}_{\text{P3HT}}}$$

# Magnetic Multilayers and Thin Films



Remarkably detailed information about magnetic structure on an inter-atomic length scale can be obtained from polarized neutron reflection and diffraction studies. (Polarized neutron reflection data on magnetic semiconductor superlattices by Henryk Kepa et al.)

# Bibliography / References

Optics, 3rd Ed., by E. Hecht, Addison-Wesley, 1998.

Neutron Optics, by V.F. Sears, Oxford University Press, 1989.

Principles of Optics, 6th Ed., by M. Born and E. Wolf, Pergamon Press, 1987.

Quantum Mechanics, 2nd Ed., by E. Merzbacher, Wiley, 1970.

“Structural Investigations of Membranes in Biology by Neutron Reflectometry”, C.F.Majkrzak, N.F.Berk, S.Krueger, and U.A.Perez-Salas, Chapter 12 in *Neutron Scattering in Biology*, Edited by J.Fitter, T.Gutberlet, and J.Katsaras, (Springer, Berlin, 2006) p.225-263.

“Polarized Neutron Reflectometry”, C.F.Majkrzak, K.V.O'Donovan, and N.F.Berk, Chapter 9 in *Neutron Scattering from Magnetic Materials*, Edited by T.Chatterji, (Elsevier, Amsterdam, 2006) p.397-471.

“Phase-Sensitive Neutron Reflectometry”, C.F.Majkrzak, N.F.Berk, and U.A.Perez-Salas, *Langmuir* **19**, 7796 – 7810 (2003).

B.J.Kirby et al., Phase-sensitive specular neutron reflectometry . . ., *Current Opinion in Colloid & Interface Science* **17** (2012) 44-53.

C.F.Majkrzak et al., *J. Appl. Phys.* **110** (2011).

[www.ncnr.nist.gov](http://www.ncnr.nist.gov) -- look here for information about neutron reflectometry in general as well as in specific studies highlighted in past and current annual reports for the facility.